Investigation of biofilm expansion in *Streptococcus mutans* through EPS osmotic behavior and hydroxyapatite interactions

Moon, Jeongmi

Department of Applied Life Science
Graduate School
Yonsei University

Investigation of biofilm expansion in *Streptococcus mutans* through EPS osmotic behavior and hydroxyapatite interactions

Advisor Kwon, Jae-Sung

A Dissertation Submitted

to the Department of Applied Life Science

and the Committee on Graduate School

of Yonsei University in Partial Fulfillment of the

Requirements for the Degree of

Doctor of Dental Science

Moon, Jeongmi

June 2025

Investigation of biofilm expansion in *Streptococcus mutans* through EPS osmotic behavior and hydroxyapatite interactions

This Certifies that the Dissertation of Moon Jeongmi is Approved

Committee Chair	**Choi, Sung-Hwan**
Committee Member	**Kwon, Jae-Sung**
Committee Member	**Lee, Eun-Jung**
Committee Member	**Mangal, Utkarsh**
Committee Member	**Seo, Kyoungjin**

Department of Applied Life Science
Graduate School
Yonsei University
June 2025

TABLE OF CONTENTS

LIST OF FIGURES

LIST OF TABLES

ABSTRACT

Investigation of biofilm expansion in *Streptococcus mutans* through EPS osmotic behavior and hydroxyapatite interactions

Dental caries remains a significant global public health challenge affecting individuals across all age groups. *Streptococcus mutans* (*S. mutans*) is widely recognized as a keystone pathogen in dental caries development. However, the mechanisms by which this non-motile bacterium rapidly colonizes tooth surfaces and forms cariogenic biofilms remain incompletely understood. Previous studies have demonstrated that biofilms of both motile and non-motile bacteria can expand through osmotic pressure-mediated processes. This study aimed to investigate the osmotic pressure-mediated expansion patterns of *S. mutans* biofilms and identify key physical and chemical factors contributing to spatial expansion across tooth surfaces.

To analyze osmotic effects mediated by extracellular polymeric substances (EPS) within *S. mutans* biofilms, an abiotic model system utilizing dextran solutions was employed. Fluorescent nanoparticles were used to track water movement into the biofilm matrix. Additionally, pH changes resulting from acid production by *S. mutans* were measured, and planktonic bacterial growth analyses under various acidic conditions were conducted to evaluate the effects of acidic environments and hydroxyapatite on bacterial growth and colony formation. To characterize *S. mutans* biofilms under different nutritional conditions, an air-solid interface model with semipermeable membranes was utilized on agar plates supplemented with 1% glucose, 1% sucrose, or 1% sucrose with 1% hydroxyapatite. Biofilm development was evaluated over 6 days using stereomicroscopy and image analysis, focusing on expansion patterns, EPS production, and microcolony formation.

Results revealed that *S. mutans* biofilms expand through a unique two-stage process, distinct from expansion mechanisms observed in other bacterial species. The EPS model experiments demonstrated increased height and spreading of dextran solutions due to water absorption from surrounding agar media, indicating sufficient osmotic pressure formation to drive outward EPS flow. Viable bacteria were confirmed within the EPS matrix, demonstrating that the matrix serves as a vehicle for bacterial transport to new locations. Planktonic growth analyses showed significant growth inhibition under acidic conditions, confirming that the buffering capacity of hydroxyapatite is essential for stable *S. mutans* biofilm colony formation.

Analysis of *S. mutans* biofilm expansion patterns showed that only biofilms grown in media containing both sucrose and hydroxyapatite exhibited significant expansion. In contrast, biofilms grown in media containing only glucose or sucrose showed no significant expansion despite daily media replacement. Under conditions containing both sucrose and hydroxyapatite, EPS matrix spread outward due to osmotic pressure, followed by new colony formation in hydroxyapatite-containing environments. Microcolony analysis within biofilms revealed distinct morphological

differences based on distance from the initial inoculation site. Colony size increased with distance from the original inoculation zone, confirming gradually improving growth conditions with increasing distance.

In conclusion, this study demonstrated a novel two-stage expansion process in *S. mutans* biofilms involving osmotic pressure-driven EPS matrix spreading followed by new colony formation in hydroxyapatite-containing environments. This expansion pattern differs from conventional biofilm development mechanisms and explains how non-motile *S. mutans* biofilms can rapidly colonize tooth surfaces in sucrose-rich environments. The essential roles of EPS osmotic properties and environmental pH regulation provide new insights into cariogenic biofilm behavior and present additional scientific evidence for developing prevention and treatment strategies targeting EPS. This research advances understanding of cariogenic biofilm development and is expected to contribute to establishing effective preventive strategies against dental caries.

Key words : Cariogenic biofilm, *S. mutans*, Biofilm expansion, EPS, Osmotic pressure

1. INTRODUCTION

1.1. Dental caries

Dental caries is a common and one of the most prevalent chronic dental diseases that affects two billion people worldwide (Cheng et al. 2022; Pitts et al. 2017), and 514 million of them are children (World Health Organization 2022). Despite advances in preventive dentistry, dental caries remain pervasive across all age groups, socioeconomic levels, and geographic regions (World Health Organization 2022). This widespread condition is a localized dental issue and a significant public health challenge affecting overall well-being and quality of life. Dental caries range from initial enamel demineralization to extensive cavitation of teeth. When left untreated, caries can lead to further implications, including pulpal inflammation and systemic infection (Rathee and Sapra 2023). Furthermore, dental caries tends to affect socioeconomically disadvantaged groups more, highlighting the significance of the disease (Dye et al. 2017; Reisine and Psoter 2001; Schwendicke et al. 2015). For such reasons(World Health Organization 2022), numerous studies have been conducted to prevent and treat dental caries. The continuing high prevalence(World Health Organization 2022), however, indicates that further understanding of dental caries, especially at the microbiological level, is essential for developing more effective preventive and therapeutic strategies.

1.2 Etiology and pathogenesis of dental caries

Dental caries is a multifactorial disease characterized by the progressive demineralization of tooth structure (Cawson and Odell 2008; Pitts et al. 2017; Selwitz, Ismail, and Pitts 2007). This chronic condition involves complex interactions among host factors, dietary components, and the oral microbiome (Pitts et al. 2017; Selwitz, Ismail, and Pitts 2007). The process of dental caries begins when acids produced by the oral microbiome cause the pH to drop below the critical threshold of 5.5. At this acidity level, hydroxyapatite ($Ca_{10}(PO_4)_6(OH)_2$), the crystalline form of calcium phosphate that primarily composes teeth, begins to dissolve (Manton and Hayes-Cameron 2013; Selwitz, Ismail, and Pitts 2007).

The dissolution process initially occurs at the nanoscale, particularly at crystal defect sites and prism boundaries. As hydroxyapatite dissolves, it releases calcium and phosphate ions into the surrounding fluid. This early demineralization manifests clinically as white spot lesions, representing localized areas of decreased mineral content, although the surface remains relatively intact (Selwitz, Ismail, and Pitts 2007). Without intervention, continuous exposure to acidic conditions leads to progressive mineral loss. The subsurface demineralization continues, eventually resulting in surface breakdown and the formation of cavities (Pitts et al. 2017; Selwitz, Ismail, and Pitts 2007)

The traditional understanding of caries etiology centers on the plaque hypothesis, which states that changes in environmental conditions favor the growth of aciduric and acidogenic bacteria, leading to dysbiosis in the balanced oral microbiome (Pitts et al. 2017; Selwitz, Ismail, and Pitts 2007). This dysbiosis is primarily triggered by frequent dietary carbohydrate exposure, which provides a substrate for acid production by cariogenic bacteria (Selwitz, Ismail, and Pitts 2007; Sheiham and James 2014). The acidic environment that develops further favors the growth of aciduric microorganisms, reinforcing the pathogenic cycle (Takahashi 2005). Building on this understanding, prior studies have predominantly explored environmental modifications, including dietary control and the use of fluoride, as key strategies for managing oral biofilm development (Cawson and Odell 2008; Manton and Hayes-Cameron 2013).

Among numerous bacterial species that have been studied in caries research, *Streptococcus mutans* (*S. mutans*) is recognized as a key pathogen due to its acidogenicity, acid tolerance, and ability to synthesize extracellular polymeric substances (EPS) that enhance biofilm formation and structural integrity (Bowen et al. 2018; Selwitz, Ismail, and Pitts 2007). *S. mutans* adheres to tooth surfaces and contributes to enamel demineralization by synthesizing EPS and organic acids as metabolic byproducts (Bowen et al. 2018; Flemming et al. 2016; Koo et al. 2017; Manton and Hayes-Cameron 2013). The localized acid production by *S. mutans* within the biofilm drops pH below the critical threshold of 5.5, causing demineralization of tooth (Colombo and Tanner 2019; Heng 2016; Larsen and Fiehn 2017; Mira, Simon-Soro, and Curtis 2017). Therefore, elucidating the

underlying processes of cariogenic biofilm formation and proliferation is crucial for developing targeted interventions against dental caries.

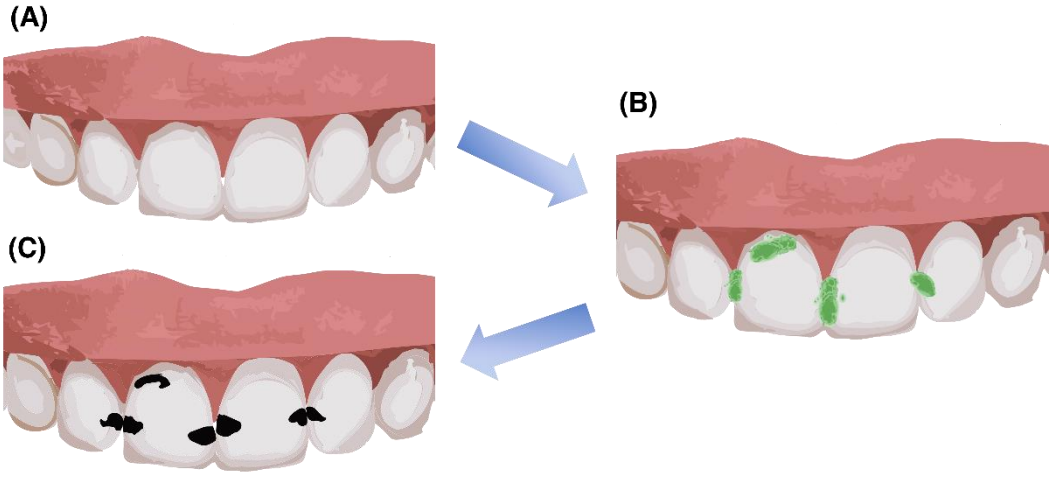

<Fig 1> Schematic illustration of dental caries process. (A) Healthy teeth. (B) Cariogenic biofilm formed on teeth. (C) Dental caries.

1.3 *Streptococcus mutans* as a keystone pathogen

Biofilm formation in the oral cavity follows a sequential process. It begins with the adsorption of salivary proteins and lipids onto the tooth surface, forming the acquired pellicle within minutes of cleaning (Scannapieco 1994). The acquired pellicle alters surface properties and provides specific receptors for bacterial adhesion (Cisar et al. 1997). Initial colonization occurs as planktonic bacteria attach to the pellicle through weak, reversible physicochemical interactions, followed by stronger, irreversible adhesion mediated by specific bacterial adhesins (Cisar et al. 1997; Scannapieco 1994).

As bacteria colonize and proliferate, they secrete EPS, forming the biofilm matrix's scaffold. EPS are biopolymers primarily composed of exopolysaccharides, proteins, lipids, and extracellular DNA (Flemming and Wingender 2010). As the biofilm matures, bacterial cells organize into complex three-dimensional structures.

In cariogenic biofilms, EPS production is significant as it contributes to bacterial accumulation, acid production, and retention on the tooth surface. The maturation of cariogenic biofilm is accompanied by ecological shifts driven by frequent exposure to dietary carbohydrates (Flemming et al. 2023; Koo, Falsetta, and Klein 2013). These environmental changes favor acidogenic and aciduric species, increase EPS production, and develop acidic microenvironments that initiate the demineralization process characteristic of early caries lesions (Colombo and Tanner 2019; Heng 2016; Larsen and Fiehn 2017; Mira, Simon-Soro, and Curtis 2017).

S. mutans is a keystone pathogen in cariogenic biofilm due to its virulence factors that contribute to caries initiation and progression (Pitts et al. 2017). It was first isolated by J.K. Clarke in 1924 from carious lesions (Clarke 1924). By the mid-1960s, clinical and animal studies identified *S. mutans* as a keystone species for dental caries (Lemos and Burne 2008). *S. mutans* is Gram-positive, facultatively anaerobic, and has cariogenic properties.

The virulence of *S. mutans* includes its ability to adhere to tooth surfaces through sucrose-dependent and sucrose-independent mechanisms (Berne et al. 2018). It expresses multiple adhesins, including antigen I/II (AgI/II), which enables initial attachment to salivary glycoproteins in the acquired pellicle (Lemos et al. 2019; Manzer, Nobbs, and Doran 2020). Additionally, glucosyltransferases (GtfB, GtfC, and GtfD) from *S. mutans* adsorb to both pellicle-coated and uncoated hydroxyapatite surfaces in an active form, enabling in situ glucan synthesis that enhances bacterial adhesion and biofilm accumulation (Lemos et al. 2019).

S. mutans can metabolize a wide range of carbohydrates, which plays a crucial role in its cariogenic potential (Lemos et al. 2019). This is facilitated by multiple phosphoenolpyruvate-dependent sugar phosphotransferase systems (PTS) and ATP-binding cassette (ABC) transporters, allowing efficient uptake and utilization of various monosaccharides and disaccharides (Lemos et al. 2019). Among these, sucrose is particularly important, serving as an energy source and a substrate

for exopolysaccharide synthesis (Bowen and Koo 2011; Klein et al. 2015; Lemos et al. 2019). Unlike many other Gram-positive bacteria that rely on the CcpA-dependent pathway for carbon utilization, *S. mutans* primarily regulates carbohydrate metabolism through the glucose/mannose-PTS system (Lemos et al. 2019).

The acidogenic nature of *S. mutans* plays a central role in developing dental caries. By fermenting dietary carbohydrates, it produces organic acids, primarily lactic acid, as byproducts (Lemos et al. 2019; Zeng and Burne 2013). When the pH drops below the critical threshold of 5.5, enamel demineralization occurs, initiating the caries process. Unlike many competing oral bacteria that become metabolically inactive in acidic conditions, *S. mutans* continues to metabolize carbohydrates and produce acid, giving it a selective advantage (Lemos et al. 2019). The persistent acidification shifts the dental plaque microbiome toward a more acidogenic and cariogenic composition, further reinforcing its role in cariogenic biofilm.

Other than acidogenic properties, the acid tolerance of *S. mutans* is another key factor in cariogenic biofilm (Baker, Faustoferri, and Quivey 2017; Lemos et al. 2019). When exposed to low pH, *S. mutans* initiates an acid tolerance response (ATR), employing various adaptive mechanisms to maintain intracellular pH homeostasis. Central to this response is the membrane-bound F_1F_o-ATPase, which actively pumps protons out of the cell and functions optimally at pH 6.0 (Kuhnert et al. 2004; Sheng and Marquis 2006). To further protect itself, *S. mutans* alters its membrane composition to reduce proton permeability by increasing monounsaturated fatty acids and elongating carbon chains (Fozo and Quivey 2004). Additionally, cytoplasmic buffering is achieved through the agmatine deiminase system (AgDS) and carbonic anhydrase-mediated conversion of CO_2 to bicarbonate (Griswold, Chen, and Burne 2004). These mechanisms work together, allowing *S. mutans* to remain viable under acidic conditions, reinforcing its role as a primary driver of dental caries.

1.4. Bacteria biofilm spreading

Biofilms represent organized microbial communities that are encased within a self-generated extracellular polymeric substance (EPS) matrix, which includes exopolysaccharides, proteins, extracellular DNA (eDNA), and lipids. This hydrated, viscoelastic matrix provides structural integrity, protects cells from environmental stresses, and facilitates spatial organization. Biofilms can form on various surfaces such as teeth, medical devices, and mucosal tissues (Flemming et al. 2023; Flemming and Wingender 2010; Karygianni et al. 2020). Understanding this architectural framework is essential for interpreting the mechanisms underlying biofilm expansion across the tooth surface.

The expansion of cariogenic biofilms across tooth surfaces has significant clinical implications, as it facilitates the initiation of multiple carious lesions and contributes to the progression of existing demineralization zones. Understanding how these biofilms spread is crucial for developing effective preventive and therapeutic strategies. Previously, pathogenic bacteria have been reported to spread through several mechanisms, including motility (Kearns 2010), physical contact (Berkowitz and Jones 1985), and transmission via fluids (Hall-Stoodley and Stoodley 2005). In dental caries, the initial acquisition of cariogenic bacteria follows a vertical transmission pattern, primarily from mother to child, during a specific "window of infectivity" around two years of age when primary dentition is fully erupted (Caufield, Li, and Dasanayake 2005). Genetic studies have confirmed this mother-to-child transmission, with research showing over 70% of children carry *S. mutans* strains identical to their mothers (da Silva Bastos Vde et al. 2015). However, these mechanisms fall short of explaining biofilm expansion in non-motile species such as *S. mutans*, highlighting the need to reconsider biofilm development.

In general, conventional pathogenic biofilm expansions have predominantly explained via bacterial growth and active motility. Motile bacteria like *Pseudomonas aeruginosa* utilize flagella-mediated swimming and twitching motility via type IV pili to colonize surfaces efficiently (Bru et al. 2023; Kearns 2010). These active motility systems enable individual bacteria or bacterial aggregates to translocate across surfaces, facilitating the colonization of new territories and the expansion of the biofilm boundary (Fig 2A). In the oral environment, while some periodontal pathogens employ similar strategies (Ji, Choi, and Choi 2015), these fail to explain biofilm expansion in non-motile organisms like *S. mutans*, suggesting a need for a paradigm shift in biofilm research.

Recent advances in biofilm research have revealed that physical processes independent of bacterial motility can drive biofilm expansion (Jautzus, van Gestel, and Kovács Á 2022; Seminara et al. 2012; Yan et al. 2017). Yan et al. showed genetically modified non-motile *Vibrio cholerae* facilitates biofilm spreading through the production of EPS, generating osmotic pressure gradients (Yan et al. 2017) (Fig 2B). Seminara et al. also showed that *Bacillus subtilis* utilizes osmotic

pressure-mediated biofilm spreading rather than its own motility (Seminara et al. 2012).

As bacteria within the biofilm synthesize matrix components, the increasing osmotic pressure causes the biofilm to swell and spread outward (Bru et al. 2023; Jautzus, van Gestel, and Kovács Á 2022; Maier 2021; Seminara et al. 2012; Trinschek, John, and Thiele 2016; Yan et al. 2017). This paradigm shift in understanding biofilm expansion provides a potential explanation for non-motile oral bacteria like *S. mutans* efficiently colonizing tooth surfaces despite lacking conventional motility structures.

Osmotic pressure-mediated biofilm spreading begins with bacteria consuming water and nutrients and producing EPS. As EPS accumulates within the biofilm, it creates a polymer-rich environment where these large molecules cannot freely diffuse out (Seminara et al. 2012; Yan et al. 2017). This concentration gradient establishes an osmotic imbalance between the biofilm and its surroundings.

The resulting osmotic pressure difference draws water from the moist substrate into the biofilm (Seminara et al. 2012). Initially, this water influx causes the biofilm to predominantly expand vertically as it swells to equilibrate the osmotic pressure (Seminara et al. 2012; Trinschek, John, and Thiele 2016). This vertical growth continues until the biofilm reaches a critical height. The biofilm then transitions from vertical swelling to horizontal spreading (Seminara et al. 2012; Trinschek, John, and Thiele 2016). The osmotic pressure gradient becomes most pronounced at the colony edges, redirecting the expansion laterally rather than upward (Seminara et al. 2012; Trinschek, John, and Thiele 2016).

This physical expansion driven by osmotic pressure gradients involves two complementary mechanisms: passive swelling and enhanced cell growth (Yan et al. 2017). Passive swelling happens directly as water enters the biofilm in response to osmotic forces. Simultaneously, the influx of nutrients stimulates the growth of peripheral cells, which produce additional EPS, sustaining the cycle of osmotic pressure-driven expansion (Seminara et al. 2012; Yan et al. 2017).

To date, no studies have examined whether the non-motile *S. mutans* biofilm can expand across surfaces through osmotic pressure. The dynamic oral environment caused by frequent nutrient intake and humid conditions differs from the environments of previously studied non-motile bacteria. Furthermore, *S. mutans*' distinctive acid production may result in expansion patterns unlike the previously studied non-motile biofilms.

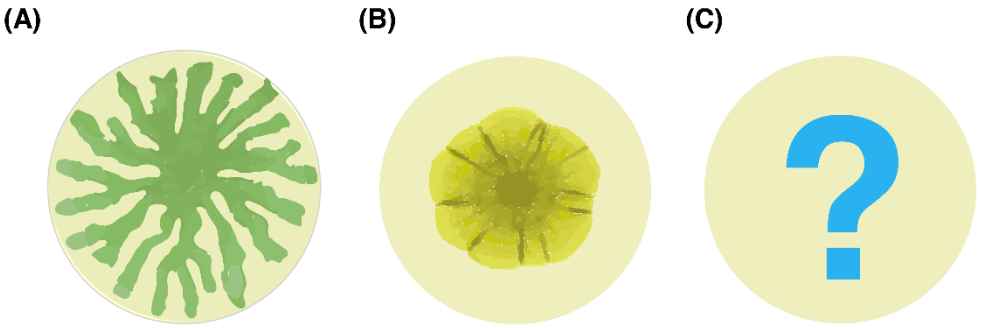

<Fig 2> Schematic illustration of biofilm expansion. (A) Expansion of motile biofilm on agar surface (e.g. *Pseudomonas aeruginosa*). (B) Osmotic pressure-driven expansion of non-motile, non-oral biofilm (e.g. genetically modified non-motile *Vibrio cholerae)*. (C) Expansion of non-motile *S. mutans* biofilm remains unknown.

1.5. The role of Extracellular Polymeric Substances (EPS)

The concept of EPS has evolved considerably from early observations of microbial "slime" (Flemming 2016). Beckwith identified polysaccharides in microbial accumulation (Beckwith 1931). Later, it was found to have a complex composition, including exopolysaccharides, proteins, nucleic acids, and lipids (Wingender, Neu, and Flemming 1999). Advanced visualization techniques revealed the matrix's structure (Lawrence et al. 2007), showing a highly organized scaffold (Flemming 2011). EPS constitutes a critical component of cariogenic biofilms, accounting for approximately 50-95% of the biofilm dry mass (Saini, Saini, and Sharma 2011). EPS plays multifaceted roles within cariogenic biofilms that significantly enhance virulence and contribute to disease progression.

First, EPS enhances bacterial adherence to tooth surfaces by binding sites for initial colonization. Surface-adsorbed Gtfs rapidly form a layer of exopolysaccharides that promote the attachment of *S. mutans* and other oral bacteria (Schilling and Bowen 1992).

Second, EPS provides structural integrity and mechanical stability to the biofilm. EPS serves as a scaffold for bacterial cells, allowing for the development of microcolonies and supporting their continuous growth (Xiao and Koo 2010).

Third, the EPS matrix creates protective environments that shield bacterial cells from antimicrobial agents and environmental stress. The dense network of polymers limits diffusion, reducing the penetration of antimicrobials and contributing to the increased resistance of biofilm bacteria to antimicrobials compared to planktonic bacteria (Flemming et al. 2023; Flemming and Wingender 2010).

Fourth, some EPS functions as an extracellular energy reservoir. During periods of nutrient deprivation, these polymers can be metabolized by bacteria, providing a competitive advantage for survival in the dynamic oral environment (Burne et al. 1996; Cugini et al. 2019; Karygianni et al. 2020).

Fifth, EPS influences the diffusion properties within the biofilm and limits the movement of substances into and out of the matrix. This restricted diffusion leads to the development of acidic microenvironments within the biofilm. The persistence of these low pH conditions promotes the selection of aciduric and acidogenic bacteria, further enhancing the cariogenicity of the biofilm (Hwang et al. 2016; Marsh 2003).

Understanding the complex roles of EPS in biofilm formation and pathogenicity is essential for developing effective strategies to prevent and control dental caries and other biofilm-associated oral diseases. Beyond the functions mentioned above, recent evidence suggests that the accumulation of EPS also influences biofilm expansion dynamics through mechanisms distinct from bacterial growth or motility (Jautzus, van Gestel, and Kovács Á 2022; Seminara et al. 2012; Yan et al. 2017).

1.6. Glucan production in *S. mutans* biofilm and osmotic pressure

The exopolysaccharides in biofilm vary depending on the microbial species. For example, *Pseudomonas aeruginosa* produces three major exopolysaccharides: polysaccharide synthesis locus (Psl), pellicle polysaccharide (Pel), and alginate. *Vibrio cholerae* produces Vibrio polysaccharide (VPS), and *Candida albicans* synthesizes α-mannans and β-glucans (Karygianni et al. 2020). *S. mutans* biofilms produce glucans as exopolysaccharides, a significant component of the EPS matrix (Klein et al. 2015; Koo et al. 2010; Lynch et al. 2007). Glucans comprise up to 40% of the dry weight of *S. mutans* biofilm (Bowen and Koo 2011; Koo et al. 2010; Paes Leme et al. 2006). The ability of *S. mutans* to synthesize glucans from sucrose is central to its role in biofilm formation and caries development.

Krasse first reported the importance of sucrose in biofilm formation (Krasse 1965). Subsequently, Gibbons and Banghart reported that cariogenic streptococci synthesized large quantities of exopolysaccharides, specifically from sucrose (Gibbons and Banghart 1967). Later, it was found that *S. mutans* possesses multiple glucosyltransferases (Gtfs), which synthesize glucans from sucrose (Hanada and Kuramitsu 1988). *S. mutans* has three distinct Gtfs (GtfB, GtfC, and GtfD) that produce both water-soluble and water-insoluble glucans.

GtfB synthesizes water-insoluble glucans rich in α-1,3-linkages (Bowen and Koo 2011). GtfB binds to the bacterial surface and requires primer dextran for optimal activity (Bowen and Koo 2011; Vacca-Smith et al. 1996). GtfC produces both soluble and insoluble glucans (Hanada and Kuramitsu 1988). Unlike GtfB, GtfC adsorbs to the enamel surface within the salivary pellicle and synthesizes glucans in situ (Bowen and Koo 2011; Vacca-Smith et al. 1996). These glucans further provide binding sites for bacterial adhesion (Bowen and Koo 2011; Schilling and Bowen 1992). GtfD synthesizes water-soluble glucans with predominantly α-1,6-linkages (Bowen and Koo 2011). These soluble glucans serve as primers for GtfB and act as a reserve polysaccharide that can be metabolized by bacteria (Bowen and Koo 2011; Walker, Pulkownik, and Morrey-Jones 1981).

Considering that *S. mutans* produces large quantities of glucans through glucosyltransferases as EPS components, it is reasonable to hypothesize that these polymers could generate significant osmotic pressure differences in *S. mutans* biofilms. Several studies have demonstrated that biofilms can generate osmotic pressure gradients due to EPS secretion (Jautzus, van Gestel, and Kovács Á 2022; Seminara et al. 2012; Trinschek, John, and Thiele 2016; Yan et al. 2017). Oral biofilms are also subjected to dynamic osmotic conditions, driven by fluctuations in dietary sugar availability, salivary flow rates, and microbial metabolic activity (Bowen and Koo 2011; Marsh 2006).

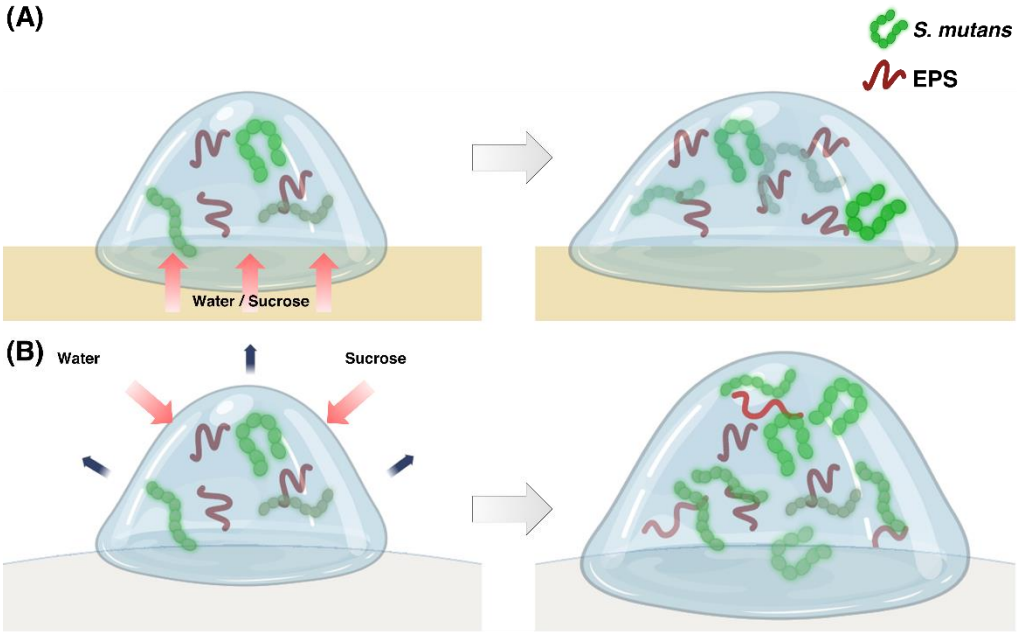

<Fig 3> Schematic representation of *S. mutans* biofilm expansion on agar and tooth surfaces. (A) On the agar surface, osmotic uptake of water and nutrients facilitates lateral biofilm expansion. (B) On the tooth surface, biofilm expansion is similarly driven by the osmotic influx of water and surrounding nutrients from the oral environment.

1.7 Possible influence of pH dynamics and hydroxyapatite interactions on *S. mutans* biofilm

Dental biofilms exist in a dynamic environment, going through pH fluctuations as *S. mutans* produces acid from metabolizing nutrients. While *S. mutans* is well-established as an aciduric bacterium capable of surviving in low-pH environments (Matsui and Cvitkovitch 2010), the relationship between environmental pH, bacterial proliferation, and hydroxyapatite dissolution presents a more complex interplay (Cieplik et al. 2020; Park, Sutherland, and Rafii 2019).

The pH of healthy oral surfaces typically ranges from 6.0 to 7.5 (Aframian, Davidowitz, and Benoliel 2006), which is a condition favorable for the growth of most oral bacteria (Jones, Cochrane, and Percival 2015). Similar to most bacteria, *S. mutans* exhibits its optimal growth and metabolic activity within neutral pH ranges, despite its aciduric properties (Matsui and Cvitkovitch 2010). Research has shown that various environmental factors, including pH, affect the growth of bacteria and biofilm formation capacity (Jones, Cochrane, and Percival 2015). The distinction between acid tolerance and optimal growth conditions is crucial for understanding biofilm dynamics, as survival capability differs from the potential for proliferation.

Hydroxyapatite ($Ca_{10}(PO_4)_6(OH)_2$), the primary mineral component of dental enamel, undergoes dissolution when exposed to acids according to the reaction (Cieplik et al. 2020):

$$Ca_{10}(PO_4)_6(OH)_2 + 14H^+ \rightarrow 10Ca^{2+} + 6H_2PO_4^- + 2H_2O$$

This dissolution process releases calcium and phosphate ions, which creates a buffering effect in the acidic environment (Cieplik et al. 2020). Although *S. mutans* is aciduric, its proliferation may be enhanced under the more neutral conditions created by this buffering effect. This suggests that the tooth structure itself may involuntarily contribute to conditions that support bacterial growth and biofilm development.

Based on the literature reviewed, the expansion of cariogenic *S. mutans* biofilms across tooth surfaces likely involves mechanisms beyond conventional bacterial motility. For non-motile organisms like *S. mutans*, the production and accumulation of glucan-rich extracellular polymeric substances (EPS) may generate osmotic pressure gradients that facilitate biofilm expansion. Furthermore, the interaction between expanding biofilms and hydroxyapatite may influence colonization patterns through modulation of microenvironments.

1.8. Research objectives

This study aims to investigate how non-motile cariogenic *S. mutans* biofilms expand through processes distinct from conventional bacterial spreading. Specifically, the objectives of this research are:

1. To investigate the role of osmotic pressure, generated by glucan-rich EPS, in facilitating the outward movement of bacterial cells within the biofilm.

2. To investigate the role of the interaction between hydroxyapatite and biofilms in facilitating biofilm expansion.

3. To investigate whether *S. mutans* biofilm expansion can occur through EPS-associated processes despite the absence of motility, as has been reported in other bacterial species.

2. MATERIALS AND METHODS

2.1. Materials

Streptococcus mutans (American Type Culture Collection [ATCC] 25175) was obtained from ATCC (Manassas, VA, USA). Fluorescent *S. mutans* (ATCC 25175/pVMTeal) was gifted by Professor Margaret Vickerman (University at Buffalo, School of Dental Medicine). All streptococcal strains were verified to be consistent with their identification by partial sodA gene sequencing and comparison to the GenBank database. Bacterial growth media used were as follows: Todd–Hewitt broth (THB, Cat. No. 249240, Difco Laboratories, Detroit, MI, USA), Mueller–Hinton broth (MHB, Cat. No. 275730, Difco Laboratories, Detroit, MI, USA), and agar (molecular genetics-grade, Cat. No. BP1423-500, Fisher Bioreagents, Fair Lawn, NJ, USA; product of Mexico). Cell culture inserts with polyethylene terephthalate (PET) membrane (0.4 μm pore size, sterile, 12-well plate format) were acquired from Celltreat Scientific Products (Pepperell, MA, USA). Sucrose (CAS No. 57-50-1, Cat. No. S5-3, Certified ACS Crystalline, Lot 223767) was obtained from Fisher Chemical (Fair Lawn, NJ, USA). Glucose (CAS No. 50-99-7, Cat. No. 16828.36), hydroxyapatite powder ($Ca_{10}(PO_4)_6(OH)_2$, CAS No. 1306-06-5), and dextran (MW 20,000, CAS No. 9004-54-0, Cat. No. J61216.22) were obtained from Sigma-Aldrich (St. Louis, MO, USA). Fluorescent nanoparticles (FluoSpheres™ carboxylate-modified microspheres, 0.02 μm, excitation/emission: 535/575 nm, Cat. No. F8784) were obtained from Invitrogen (Carlsbad, CA, USA). LIVE/DEAD™ BacLight™ Bacterial Viability Kit (Cat. No. L7007, Invitrogen), and methyl red (ACS grade, Cat. No. 036682.14, CAS No. 493-52-7) were obtained from Thermo Fisher Scientific (Waltham, MA, USA).

2.2. Instruments

A Leica M205 FA stereomicroscope (Leica Microsystems, Wetzlar, Germany) fitted with a Leica Plan APO 1.0x M series objective lens and a K5 Scientific CMOS microscope camera was used to observe *S. mutans* biofilm expansion and abiotic dextran solution spreading. The microscopic images were acquired and processed with Leica Application Suite (LAS) EZ imaging software (Leica Microsystems, Wetzlar, Germany). Nikon Eclipse Ti300 CLSM (Confocal Laser Scanning Microscopy) (Nikon Instruments Inc., Melville, NY, USA) with a Nikon C2plus camera (Nikon Instruments Inc., Melville, NY, USA) and Zeiss LSM900 laser scanning microscope (Carl Zeiss AG, Oberkochen, Germany) with Axio Observer 7 inverted microscope were used for microscopic observation. The confocal images were acquired and processed with NIS-Elements AR software and Zen Blue software (Carl Zeiss AG, Oberkochen, Germany), respectively. A Fisherbrand Accumet basic AB15 pH meter (Thermo Fisher Scientific, Waltham, MA, USA) was used to measure pH values. A microplate reader (Epoch, BioTek Instruments, Inc., Winooski, VT, USA) was used to measure the optical density of planktonic *S. mutans* suspension.

2.3. *S. mutans* growth characterization

Bacterial strains were preserved at −80 °C in sterile glycerol solution (final concentration 50%). To ensure culture purity, strains were routinely monitored based on colony morphology, Gram staining, and catalase activity. *S. mutans* was cultured in THB, streaked as single colonies on a TH agar, and incubated at 37 °C in a 5% CO_2 atmosphere for 48 hours. Formed colonies were then incubated in fresh THB until the stationary phase. To determine the bacterial growth curve and identify the stationary phase, *S. mutans* was cultured in THB at 37 °C under CO_2. The optical density at 600 nm was measured at 6, 7, 9, 18, 20, 22, 24, 26, 28, and 30 hours using a microplate reader (Epoch, BioTek Instruments, Inc., Winooski, VT, USA). Bacterial cell density was standardized by determining CFU/mL values of *S. mutans* cultures at different OD_{600} measurements. Specifically, planktonic *S. mutans* bacteria in the stationary phase were washed with sterile PBS and resuspended to targeted OD_{600} measurements and plated onto TH agar (n=3). The targeted OD_{600} was 0.001, 0.01, 0.1, 1.0, 2.0, and 10. Plates with bacteria were then incubated for 48 hours at 37 °C in a 5% CO_2 atmosphere and enumerated.

2.4. Abiotic model for EPS osmotic spreading

A highly concentrated dextran solution (48% w/v) was formulated by dissolving 480 mg of high-molecular-weight dextran powder into 1 mL of a sterile diluent comprising a 1:10 mixture of phosphate-buffered saline (PBS; 10× stock, CAS No. 7647-14-5, Cat. No. BP399-1, Fisher BioReagents, Fisher Scientific, Waltham, MA, USA) and deionized water. The solution was continuously stirred for 24 hours at room temperature to achieve complete solubilization and uniformity. Simultaneously, Mueller–Hinton (MH) agar plates with agar concentrations of 0.5%, 1%, and 2% (w/v) were prepared to modulate the underlying osmotic environment. To minimize confounding effects from substrate rigidity, sterile cell culture inserts were gently positioned on the surface of the solidified MH agar. Onto the center of each insert membrane, 3 μL of the viscous dextran solution was carefully dispensed, ensuring consistent volume and spatial application across conditions. The plates were incubated at 37 °C in a humidified incubator containing 5% CO_2, mimicking in vivo physiological conditions.

Droplet morphology and distribution were observed using a Leica M205 FA fluorescence stereomicroscope (Leica Microsystems, Wetzlar, Germany) under 2× and 5× magnifications. Droplet diameters were quantified using Adobe Photoshop 5.0 (Adobe Systems Inc., San José, CA, USA), while surface area analyses were performed using FIJI ImageJ software (NIH, Bethesda, MD, USA).

To evaluate osmotic volume changes in an abiotic system, a separate set of experiments was conducted using the same dextran solution. Here, 100 μL aliquots were applied to culture inserts placed on MH agar plates prepared with the same concentration gradients (0.5%, 1%, 2%). After a 1-hour incubation under the above-mentioned conditions, the inserts were removed and transferred to a flat surface, where the height of the dextran solution was measured to assess changes in fluid volume distribution induced by osmotic flux.

2.5. Osmotic water uptake by *S. mutans* biofilm

To assess the incorporation of fluorescent nanoparticles into *Streptococcus mutans* (ATCC 25175/pVMTeal) biofilms, a multi-stage experimental protocol was employed. The fluorescent bacterial strain was first cultured overnight and subsequently diluted in THB to an initial optical density (OD_{600}) of 0.1. The culture was allowed to grow to the mid-exponential phase (OD_{600} = 0.5), at which point it was adjusted to maintain the same OD_{600} value to standardize bacterial cell density across replicates. A 3 μL portion of the prepared bacterial suspension was dispensed onto the surface of sterile polyethylene terephthalate (PET) cell culture inserts with 0.4 μm pore membranes (12-well plate format; Celltreat Scientific Products, Pepperell, MA, USA). These inserts were carefully positioned on Mueller–Hinton (MH) agar plates supplemented with 1% (w/v) sucrose and incubated at 37 °C under 5% CO_2 for 24 hours to facilitate initial biofilm establishment. In parallel, a second set of MH agar plates containing 1% sucrose was prepared, into which fluorescent nanoparticles (FluoSpheres™ carboxylate-modified microspheres, 20 nm diameter, excitation/emission: 535/575 nm, Cat. No. F8784, Invitrogen, Carlsbad, CA, USA) were incorporated at a final concentration of 1 μg/mL.

Following the initial 24-hour biofilm development, the inserts with formed biofilms were transferred onto the nanoparticle-infused agar plates. A further incubation period of 24 hours was carried out under identical environmental conditions to promote interaction between the biofilm matrix and fluorescent particles. After incubation, the inserts were relocated onto clean glass-bottom plates to enable stable imaging. Biofilm morphology and nanoparticle localization were visualized using a Nikon Eclipse Ti300 confocal laser scanning microscope (CLSM; Nikon Instruments Inc., Melville, NY, USA). Fluorescence images were acquired using 4× and 20× objectives to capture both low- and high-resolution views, allowing detailed examination of biofilm topography and internal nanoparticle distribution.

2.6. Viable *S. mutans* bacteria in EPS matrix

To verify the presence of *S. mutans* within the EPS matrix, quantify viable cells, and rule out potential contamination, a controlled bacterial culture procedure was performed. Individual colonies of *S. mutans* were aseptically isolated from TH agar plates and inoculated into 6 mL of liquid THB medium. The inoculated broth was incubated at 37 °C in a 5% CO_2 atmosphere for 28 hours to allow the bacteria to reach the stationary growth phase. Following this, the overnight culture was diluted with fresh THB medium to an OD_{600} of 0.1, and incubated further for 3 hours until the culture reached mid-exponential phase (OD_{600} = 0.5), ensuring a metabolically active population. A 3 µL volume of this standardized bacterial suspension was then deposited onto the center of a sterile, permeable PET membrane insert (0.4 µm pore size; 12-well format, Celltreat Scientific Products, Pepperell, MA, USA). These inserts were placed on the surface of MH agar plates supplemented with 1% sucrose prepared in sterile 100 mm × 15 mm polystyrene Petri dishes with optically clear lids (Fisherbrand™, Thermo Fisher Scientific, Waltham, MA, USA). Plates were incubated at 37 °C in a humidified incubator with 5% CO_2 for 48 hours to allow sufficient biofilm and EPS matrix development. Upon completion of incubation, the surface EPS material formed directly above the original inoculation site was carefully aspirated multiple times using a 1 µL micropipette. The collected EPS was resuspended in sterile PBS, and serial dilutions were performed for colony-forming unit (CFU) enumeration. Aliquots of the diluted suspension were streaked onto fresh TH agar plates and incubated under the same environmental conditions for an additional 48 hours to quantify viable *S. mutans* cells and assess culture purity. Additionally, a portion of the same resuspended EPS sample was subjected to bacterial viability staining using the LIVE/DEAD™ BacLight™ Bacterial Viability Kit (Cat. No. L7007, Invitrogen, Thermo Fisher Scientific, Waltham, MA, USA). Fluorescent imaging was conducted using a Zeiss LSM900 confocal laser scanning microscope coupled with an Axio Observer 7 inverted platform. High-resolution images were captured using a 40× oil immersion objective and analyzed with Zen Blue software (Carl Zeiss AG, Oberkochen, Germany) to visualize and distinguish live and dead bacterial cells embedded within the EPS matrix.

2.7. pH visualization and measurements of agar plates with *S. mutans* biofilm

For pH visualization and direct measurement experiments, *S. mutans* was first cultured overnight in THB medium under controlled conditions (37 °C, 5% CO_2) until reaching the stationary phase at 28 hours. The resulting culture was diluted using fresh THB to achieve an optical density of 0.1 at 600 nm, followed by an additional 3-hour incubation period to ensure mid-exponential growth phase (OD_{600} = 0.5). Standardized bacterial suspensions (3 μL) were then carefully applied to MH agar surfaces prepared in sterile polystyrene petri dishes (60 × 15 mm, Falcon™ Bacteriological Petri Dishes with Lid, Corning Inc., Corning, NY, USA). To visually detect pH alterations, methyl red served as the pH indicator throughout these experiments. The agar medium composition included methyl red (ACS grade, Cat. No. 036682.14, CAS No. 493-52-7, Thermo Fisher Scientific, Waltham, MA, USA). Medium supplementation consisted of either 1% sucrose alone or a combination of 1% sucrose with 1% hydroxyapatite. For agar preparation, hydroxyapatite powder was added to cooled liquid agar and mixed thoroughly to ensure uniform dispersion, following aseptic techniques described by Sanders (Sanders 2012). The concentration of hydroxyapatite powder was set at 1% for all experiments based on preliminary testing. Although previous studies have used hydroxyapatite powder concentrations ranging from 0.5% to 5%, concentrations exceeding 1.5% prevented proper solidification of the agar plates, making them unsuitable for experimental use. Following bacterial inoculation, plates underwent a 10-minute equilibration period at ambient temperature to facilitate bacterial absorption into the agar before being transferred to incubation conditions (37 °C, 5% CO_2). Beyond visual pH indication, quantitative pH assessment was conducted using a Fisherbrand Accumet basic AB15 pH meter (Thermo Fisher Scientific, Waltham, MA, USA). After a 48-hour growth period, pH values were recorded in intervals (0, 5.0, 10.0, 20.0, and 30.0 mm) measured from colony peripheries. These measurements were carried out by precise electrode placement on agar surfaces at the designated measurement points.

2.8. Planktonic bacteria growth under acidic conditions

To examine the pH-dependent behavior of *S. mutans*, Mueller–Hinton Broth (MHB) was adjusted to pH 4.5, 5.5, 6.5, and 7.8 using appropriate biological buffers: acetate buffer (for pH 4.5 and 5.5), phosphate buffer (for pH 6.5), and Tris-HCl buffer (for pH 7.8). Each buffer was prepared using standard combinations of acid and conjugate base. The pH was constantly measured using a Fisherbrand Accumet Basic AB15 pH meter while agitating with magnetic stir bars. Once the desired pH was reached, MHB was dissolved in the buffered solution to a final concentration of 21 g/L and autoclaved. The pH-adjusted broth solutions were distributed into six separate 15-mL conical tubes for each experimental pH condition. Overnight *S. mutans* cultures were subsequently introduced into each pH-modified broth medium, achieving a final optical density of 0.01 at 600 nm (corresponding to approximately 10^6 CFU/mL). Following inoculation, all culture tubes were maintained under standard incubation parameters (37 °C, 5% CO_2 environment). Growth of planktonic bacteria was assessed through optical density measurements at 600 nm, recorded at designated time intervals: 0, 5, 10, 18, 24, and 28 hours following incubation initiation. To ensure statistical reliability and reproducibility, each experiment was conducted in triplicate.

2.9. Colony biofilm growth on agar plates

S. mutans colony biofilms were established on 1% MH agar plates containing various nutritional supplements. Bacterial cultures at mid-exponential growth phase (optical density at 600 nm = 0.5, equivalent to 3×10^8 CFU/mL) were used as inoculum. A 3 μL volume of bacterial suspension was deposited onto cell culture inserts equipped with polyethylene terephthalate (PET) membranes, which were then positioned on the agar surface. The experimental design incorporating PET membrane inserts was to achieve multiple objectives: (1) enable daily medium renewal without biofilm disruption, (2) ensure continuous nutrient availability, (3) prevent bacterial translocation to the underlying agar, and (4) facilitate clear microscopic visualization of biofilm architecture. MH agar was selected over the commonly used TH agar because its glucose-free formulation allows for clearer differentiation between sucrose and glucose effects on biofilm development (Jurakova et al. 2023). Individual bacterial colonies were transferred to 6 mL of liquid TH broth and cultured at 37 °C under a 5% CO_2 atmosphere for 28 hours until reaching the stationary phase. This starter culture was subsequently diluted in fresh medium to achieve an OD_{600} of 0.1, followed by 3 hours of incubation to attain mid-exponential phase (OD_{600} = 0.5). The standardized bacterial suspension (3 μL) was then carefully inoculated onto the permeable culture inserts. The 1% agar plates were prepared with different nutritional supplements: control (no additives), 1% sucrose, 1% glucose, or a combination of 1% sucrose with 1% hydroxyapatite powder. Each experimental condition included three replicate inserts per plate to ensure statistical validity. Incubation was performed at 37 °C in a 5% CO_2 environment for up to 6 days. Humidity was maintained at 90% using water-filled trays, with additional humidification achieved by co-incubating plates with sterile water-filled Petri dishes within sealed polystyrene containers (10 × 1.5 cm).

To ensure optimal growth conditions throughout the experiment, biofilm-containing membrane inserts were transferred to freshly prepared agar plates every 24 hours. Biofilm development was monitored and recorded using a Leica M205 FA stereomicroscope system, including a Leica Plan APO 1.0x objective and K5 Scientific CMOS camera. Image acquisition and processing utilized Leica Application Suite EZ software at 2× and 5× magnifications to capture comprehensive morphological data across different nutritional and environmental conditions. Biofilm dimensions were quantified using Adobe Photoshop Software 5.0 for diameter measurements, while area calculations were performed using FIJI ImageJ software (National Institutes of Health). This dual-software approach ensured accurate and comprehensive morphometric analysis of biofilm growth patterns under various experimental conditions.

2.10. Image analysis using FIJI ImageJ

Biofilm images were processed and analyzed using FIJI ImageJ software (NIH). The analysis workflow involved multiple steps to accurately identify and quantify microcolonies within the biofilm structure. Initially, automated microcolony detection was performed using the trainable Weka segmentation plugin to distinguish bacterial colonies from background areas. Following segmentation, watershed was applied, and subsequent particle analysis was conducted to extract quantitative measurements.

To ensure data quality and exclude artifacts, size-based filtering was implemented where only objects exceeding 100 μm² in area were retained for analysis, as this threshold corresponds to the minimum size of microcolonies observed in the samples. For visualization purposes, a size-based color mapping system was generated using the ROI color coder plugin within FIJI ImageJ, which assigned distinct colors to particles based on their measured areas, facilitating visual interpretation of microcolony size distribution patterns across the biofilm.

2.11. Statistical analysis

Data normality was evaluated using the Shapiro-Wilk normality test, while variance homogeneity across groups was assessed through Levene's test prior to conducting statistical comparisons. The choice of statistical tests was determined based on these preliminary assessments. For analyzing biofilm dimensions under different carbohydrate conditions (sucrose vs. glucose) and biofilm mass variations, one-way ANOVA followed by Tukey's post-hoc multiple comparison procedure was employed. When comparing bacterial counts between the initial inoculum and EPS matrix samples, Welch's modified t-test was selected. pH measurements at varying distances from biofilm colonies were analyzed using an unpaired t-test. Results are expressed as mean values with their corresponding standard deviations (mean ± SD). Statistical significance thresholds were established at $*p < 0.05$, $**p < 0.01$, and $*** p < 0.001$. All statistical tests were performed using R 4.2.2 (R Foundation for Statistical Computing, Vienna, Austria).

3. Results

3.1. Characteristics of planktonic *S. mutans* growth

The *S. mutans* growth curve exhibited distinct phases of planktonic *S. mutans* bacterial development over a 32-hour period. Fig 4 (A) shows the growth curve of *S. mutans* during 32 hours. The bacteria displayed a lag phase during the first 6 to 8 hours of incubation. Following this initial period, *S. mutans* entered an exponential growth phase that extended from approximately 8 to 24 hours. At 28 hours, the culture reached the stationary phase with a maximum optical density of approximately 0.62, after which growth plateaued. A slight decline in OD_{600} was observed after 32 hours, indicating the beginning of a death phase.

Following the growth analysis, the relationship between OD_{600} values and CFU/mL of *S. mutans* at the stationary phase was quantitatively analyzed. For each measured OD_{600} value, the corresponding CFU/mL was determined by plate counting. Fig 4 (B) shows the relationship between OD_{600} values ranging from 0.001 to 10 and the corresponding CFU/mL values ranging from 10^5 CFU/mL to 10^{10} CFU/mL on a logarithmic scale. At OD_{600} of 0.001, the measured CFU/mL was 2.3×10^5; at OD_{600} of 0.01, it was 3.3×10^6; at OD_{600} of 0.1, it was 3.6×10^7; at OD_{600} of 1.0, it was 4.5×10^8; and at OD_{600} of 10.0, it was 5.4×10^9. A clear linear relationship was observed between OD_{600} values and CFU/mL.

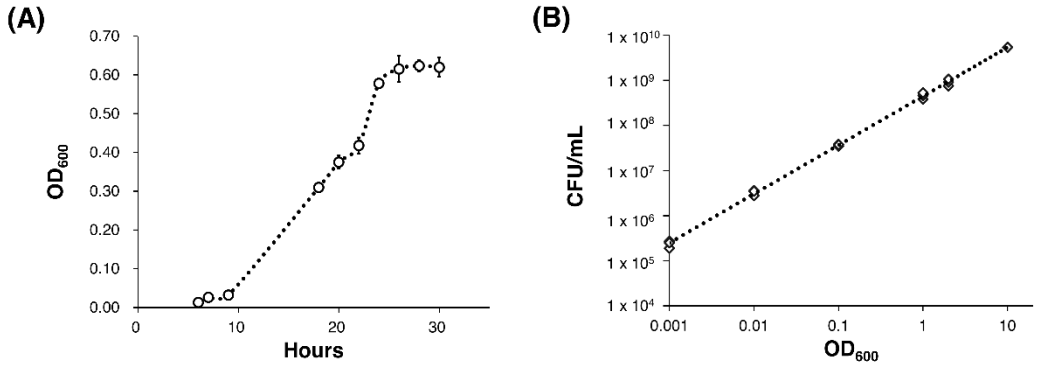

<Fig 4> Characteristics of planktonic *S. mutans*. (A) Growth curve of planktonic *S. mutans* bacteria in THB shows bacterial suspension reaching the stationary phase at 28 hours of incubation. (B) Optical density and corresponding bacterial CFU/mL of *S. mutans*.

3.2. Abiotic model for EPS osmotic spreading

The physical dynamics of EPS spreading in *S. mutans* biofilms were investigated using a dextran-based abiotic model system, where dextran solutions were applied to agar substrates of varying concentrations. Dextran droplets exhibited spreading behavior within 30 minutes across all tested agar concentrations, with expansion areas demonstrating a clear concentration-dependent pattern: 0.5% > 1% > 2% agar (Fig 5). This inverse relationship between agar concentration and droplet spreading indicated that lower agar concentrations provided greater water mobility, facilitating enhanced osmotic-driven expansion.

Osmotic pressure quantification was performed by measuring solution level changes in insert wells after 60 minutes of incubation. Hydrostatic pressure calculations were based on the observed height differences using the equation:

$$\Delta\pi=\rho\times g\times h$$

where ρ is the dextran solution density, g is gravitational acceleration, and h represents the height change between 0 and 60 minutes. The parameter Δπ corresponds to the hydrostatic pressure developed through osmotic water movement.

Measurements revealed contrasting osmotic behaviors across different agar concentrations. The 2.0% agar condition resulted in decreased solution levels, yielding negative pressure values, indicating restricted water movement within the dense gel network. Conversely, both 0.5% and 1% agar concentrations showed increased solution levels with positive pressure values, demonstrating active water uptake from the agar to abiotic dextran solution (Fig 6). These results confirmed water migration toward the concentrated dextran solution, thereby generating osmotic pressure gradients.

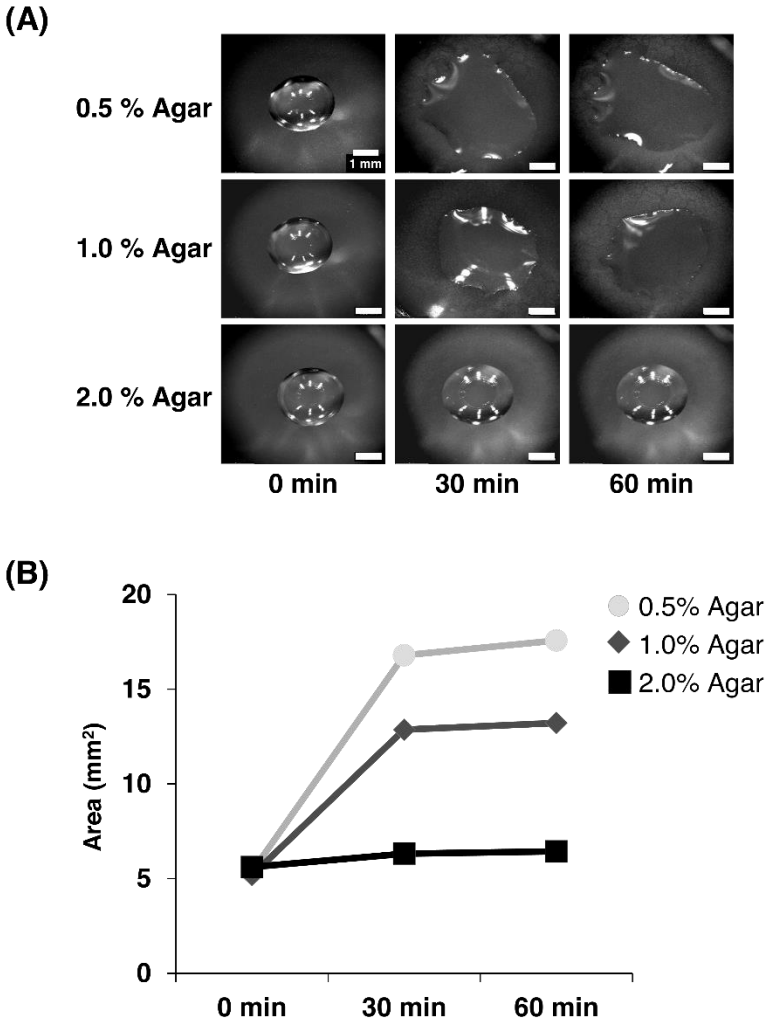

<Fig 5> Dextran solution spreads at different agar concentrations after 60 minutes. (A) Representative images of the abiotic EPS model system spreading on agar surfaces. Scale bars = 1 mm. (B) Dextran solution spread area on different agar concentrations analysed with ImageJ.

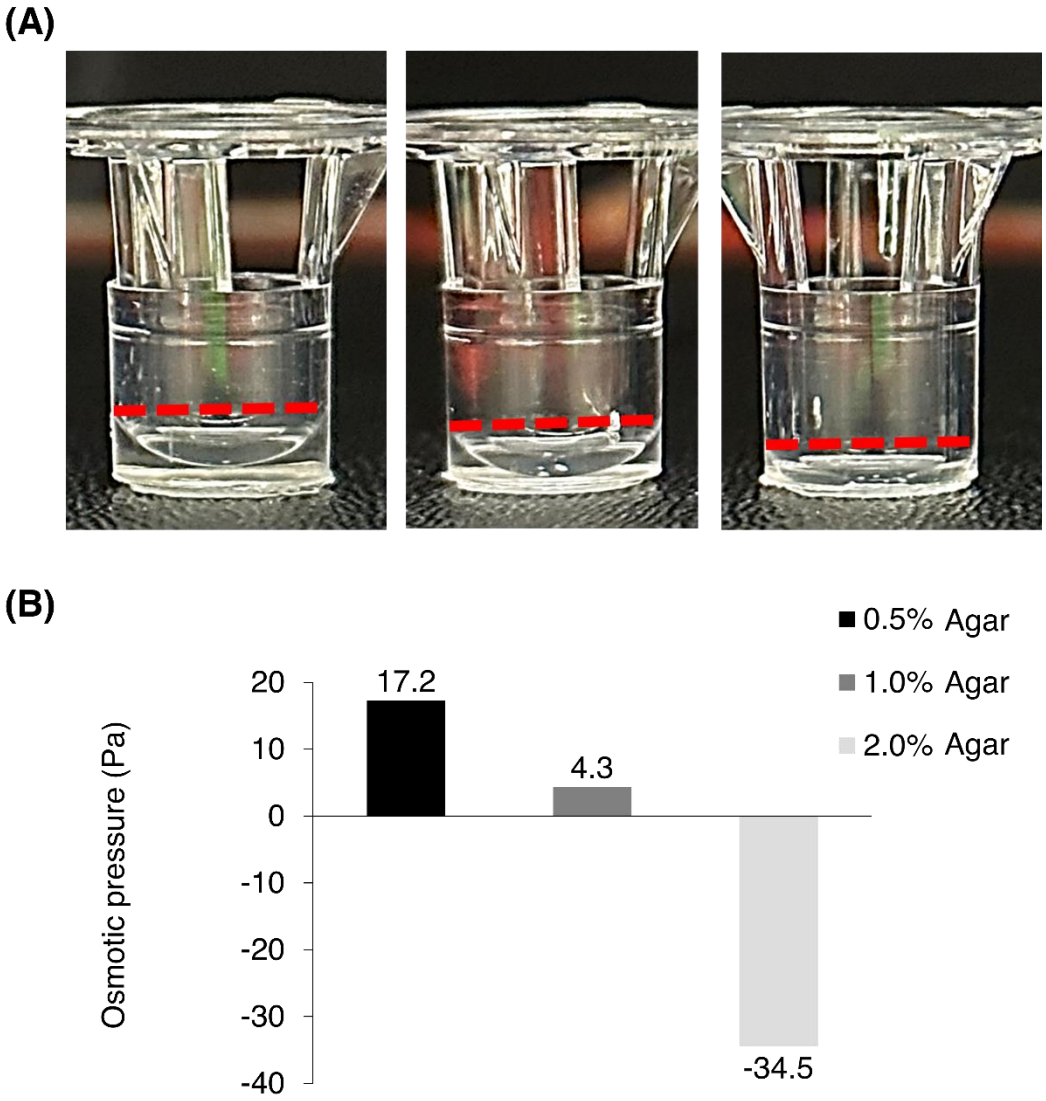

<Fig 6> Volumetric changes in dextran solution demonstrating osmotic effects across different agar substrate concentrations. (A) Images of solution height variations resulting from osmotic pressure gradients, shown from left to right: 0.5% agar, 1% agar, 2% agar substrates. (B) Quantitative analysis of dextran solution volume changes following 60-minute incubation on agar substrates of varying agar concentrations.

3.3. Osmotic water uptake by *S. mutans* biofilm

Mass differences in *S. mutans* biofilms across different agar substrate concentrations demonstrated comparable osmotic-driven phenomena, confirming findings from the dextran-based abiotic experiments. Biofilm mass measurements were conducted by comparing weights between day 2 and day 5 following a 5-day cultivation period. While statistical significance was not observed, *S. mutans* biofilms grown on sucrose-containing media exhibited mass increases that were 3-4 fold greater compared to glucose-supplemented conditions, suggesting enhanced EPS synthesis and associated water absorption (Fig 7). Biofilms cultivated on 0.5% agar substrates displayed the most pronounced mass differences.

Visualization of osmotic-driven water absorption within the EPS matrix was achieved using fluorescence microscopy with green fluorescent *S. mutans* (ATCC 25175/pVMTeal) and red fluorescent particles. Microscopic analysis revealed that green bacterial cells were consistently surrounded by red fluorescent particles (Fig 8). The red fluorescence signal extended beyond areas of direct bacterial presence, enveloping regions both with and without visible green bacteria. These observations confirmed that glucan production within the EPS matrix correlated with osmotic pressure generation and subsequent outward matrix spreading.

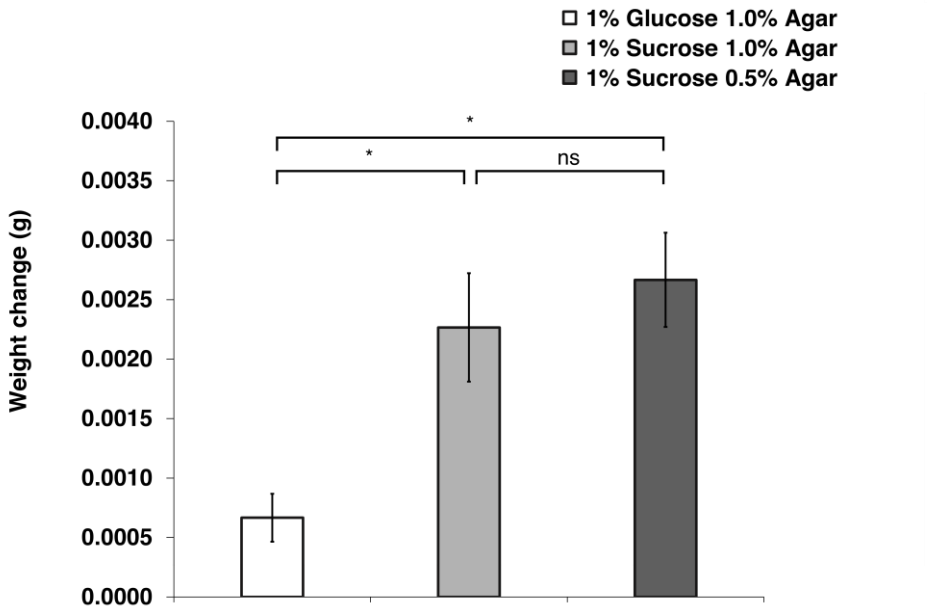

<Fig 7> Biofilm mass change of *S. mutans* after 5 days under various experimental conditions. Biofilms grown in sucrose-containing agar (1.0% and 0.5%) exhibited significantly greater water uptake compared to the glucose group ($p < 0.05$), indicating osmotic pressure–mediated absorption. No significant difference was observed between the two sucrose conditions (ns).

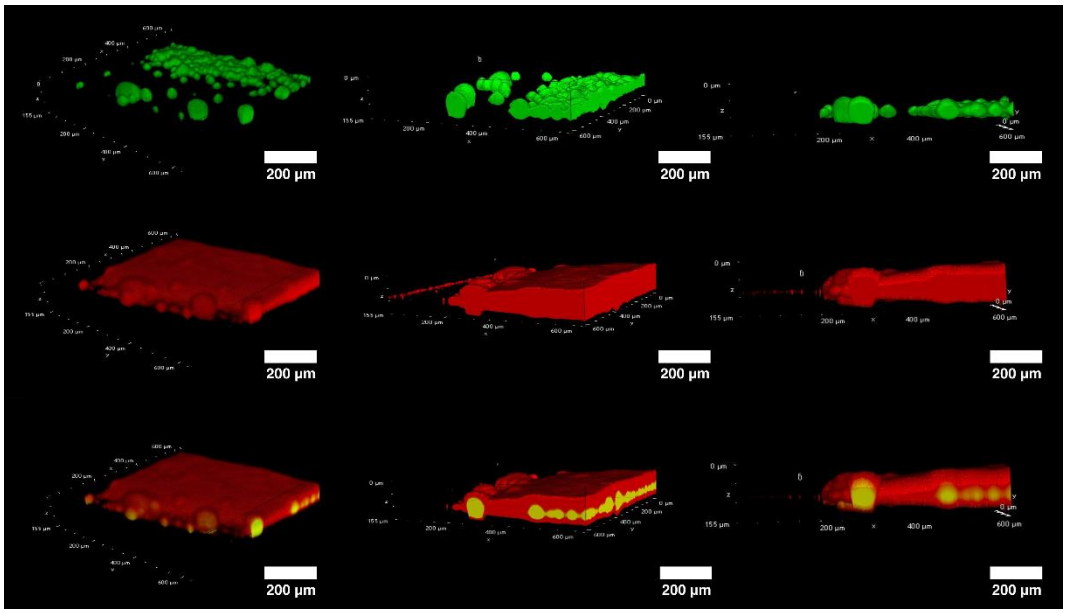

<Fig 8> CLSM images of fluorescent *S. mutans* (ATCC 25175/pVMTeal) grown on agar containing red fluorescent particles. These images demonstrate substance uptake via osmotic pressure. Green fluorescence indicates *S. mutans* colonies without additional staining (top). Red fluorescence represents the EPS matrix with red fluorescent particles that were embedded in the agar (middle). Merged image showing green *S. mutans* colonies in the red EPS matrix (bottom).
Scale bars = 200 μm.

3.4. Viable *S. mutans* bacteria in EPS matrix

To confirm EPS-mediated bacterial transport during the matrix spreading, the viability and density of bacteria within the EPS were examined. Fluorescence microscopy using LIVE/DEAD staining demonstrated distinct clusters of green-fluorescent viable bacteria distributed throughout the EPS matrix, providing evidence for bacterial survival within the spreading EPS. Quantitative bacterial enumeration revealed 5×10^6 CFU/mL within the EPS matrix, which represented a reduced population compared to the original inoculation density of 3×10^8 CFU/mL. Despite this reduction, the substantial bacterial counts within the matrix supported the microscopic observations and confirmed the bacterial transport via EPS spreading (Fig 9).

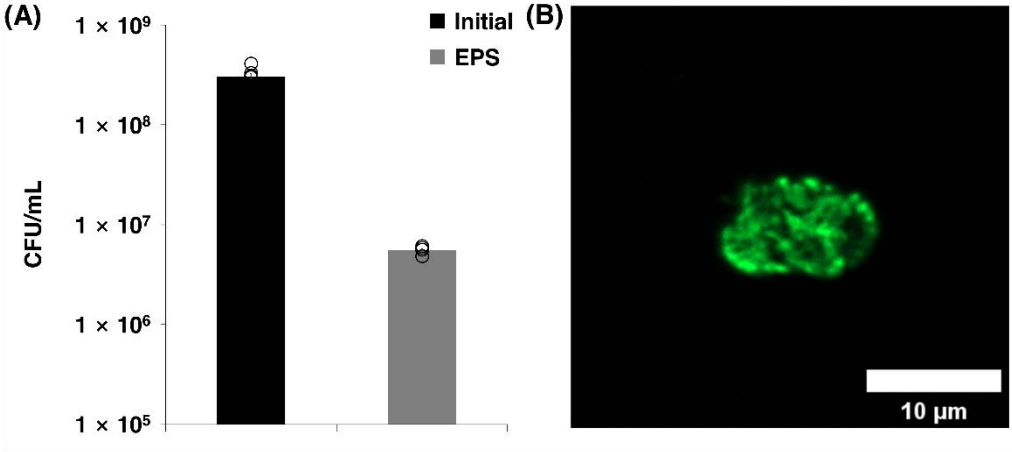

<Fig 9> Bacterial viability assessment within the *S. mutans* EPS matrix. (A) Quantitative enumeration of viable *S. mutans* recovered from EPS matrix ($p < 0.05$) (B) Confocal microscopy visualization using LIVE/DEAD staining reveals viable bacterial aggregates distributed within the EPS matrix. Scale bar = 10 μm.

3.5. pH visualization and measurements of agar plates with *S. mutans* biofilm

Hydroxyapatite's influence on environmental pH was assessed using both visual pH indicator methods and direct pH electrode measurements around the bacterial colonies. Prior to bacterial introduction, all agar plates maintained a consistent initial pH of 7.6 across experimental conditions. Following a 48-hour incubation period, pH indicator demonstrated a color shift to red in areas surrounding the biofilm, representing acidification below pH 6.2. In contrast, agar plates containing hydroxyapatite powder exhibited minimal color alterations and displayed clear, transparent zones beneath and around the biofilm (Fig 10). Direct pH measurements revealed that biofilm colonies grown without hydroxyapatite achieved a central pH of 5.7, representing a statistically significant reduction compared to hydroxyapatite-supplemented conditions ($p<0.001$). This pH differential remained significant even at distances of 5 mm from the biofilm center, extending beyond the visible biofilm perimeter, where notable differences persisted between sucrose-only and hydroxyapatite-containing groups ($p<0.05$).

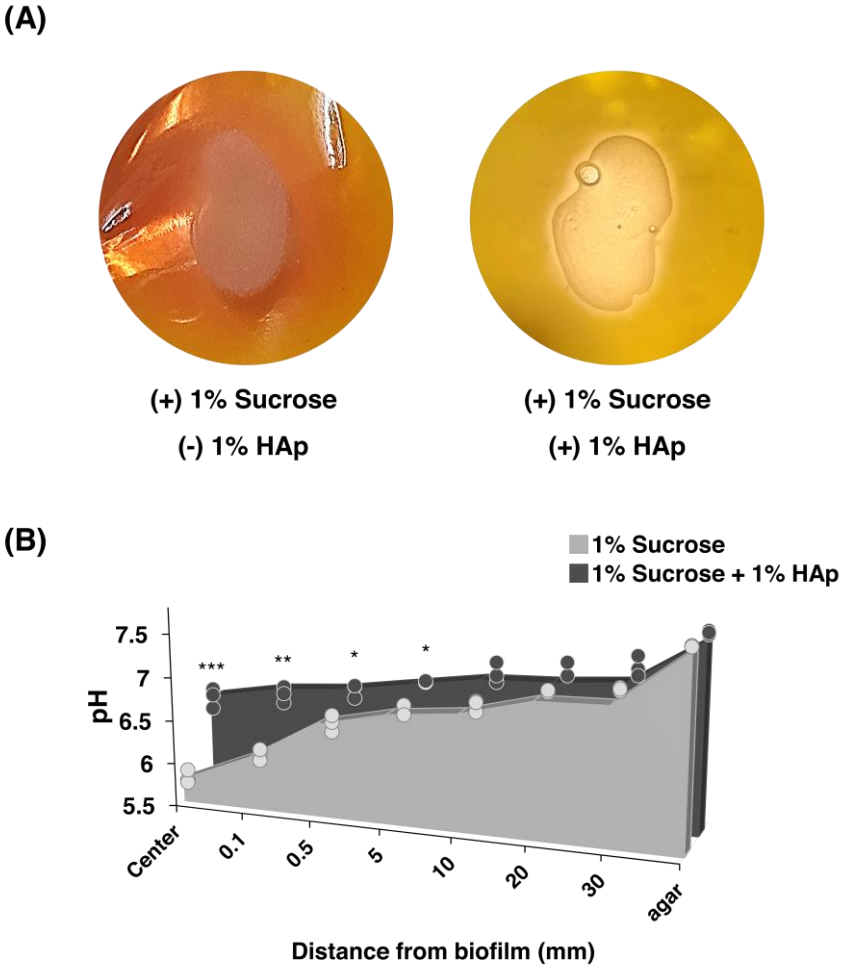

<Fig 10> Analysis of acid production by *S. mutans* biofilms and pH modulation under different substrate conditions. (A) Visual pH indicator (methyl red) demonstrates acidification (red coloration) caused by *S. mutans* metabolic acid production (left), while hydroxyapatite powder (HAp)-containing substrates show minimal pH indicator response, with transparent zones around the biofilm (right). (B) Quantitative pH measurements reveal significant acidification near *S. mutans* biofilms in the absence of hydroxyapatite, with statistical significance indicated (*$p < 0.05$, **$p < 0.01$, ***$p < 0.001$).

3.6. Planktonic bacteria growth under acidic conditions

Planktonic *S. mutans* exhibited pH-dependent growth patterns with variations observed across different acidic environments (Fig 11). Statistical analysis revealed significant growth differences between acidic and neutral conditions beginning at 5 hours post-inoculation ($p<0.001$), with these differences becoming more pronounced at the 28-hour maximum growth phase where all experimental groups demonstrated statistically significant variations ($p<0.001$). Quantitative assessment showed that bacterial growth rates and peak growth densities were diminished by approximately 40% when cultured at pH 6.5 or below relative to neutral pH conditions. Optimal bacterial proliferation was observed in neutral broth environments, whereas cultures grown at pH 4.5 demonstrated minimal growth activity throughout the 28-hour observation period. The most severe acidic conditions resulted in substantially impaired growth compared to pH 5.5 treatments ($p<0.001$).

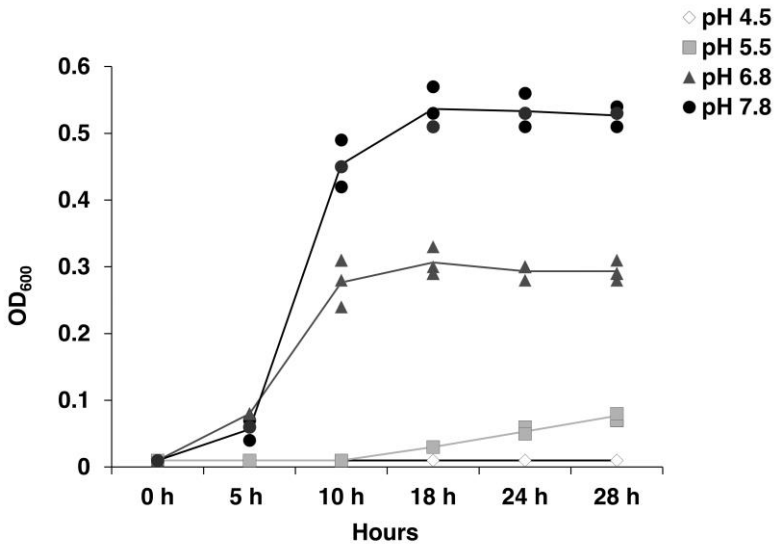

<Fig 11> Growth kinetics of planktonic *S. mutans* across varying pH environments demonstrating pH-mediated growth inhibition. Statistical analysis indicates significant growth variations among all experimental groups with the exception of pH 4.5 and 5.5 conditions during the initial 5-hour incubation period ($p<0.001$). Growth differentiation between pH 4.5 and 5.5 treatments achieved statistical significance following 24 hours of cultivation ($p<0.05$).

3.7. *S. mutans* biofilm growth on agar plates

3.7.1 Comparative analysis of biofilm development under different nutrient conditions

Observation of *S. mutans* biofilm under various nutrient conditions exhibited distinct morphological differences (Fig 12). Following overnight incubation, all agar plates produced microscopic colony biofilms. Yet, biofilms grown on various supplemented agar plates showed developmental differences during the 6-day observation period. Biofilms on agar plates supplemented with 1% glucose exhibited no significant size change or expansion over 6 days. These colonies appeared relatively uniform without visible EPS formation. Similarly, biofilms on 1% sucrose-supplemented agar maintained their initial size without significant expansion, despite producing visible EPS. Even under high humidity conditions, sucrose-only biofilms showed EPS matrix spreading but failed to form new colonies beyond the initial inoculation site. Only biofilm grown on agar plates supplemented with 1% sucrose and 1% hydroxyapatite powder showed expansion within 6 days with a unique pattern (Fig 17). The expansion of *S. mutans* biofilm under this condition showed EPS matrix outflow, followed by subsequent colony formation.

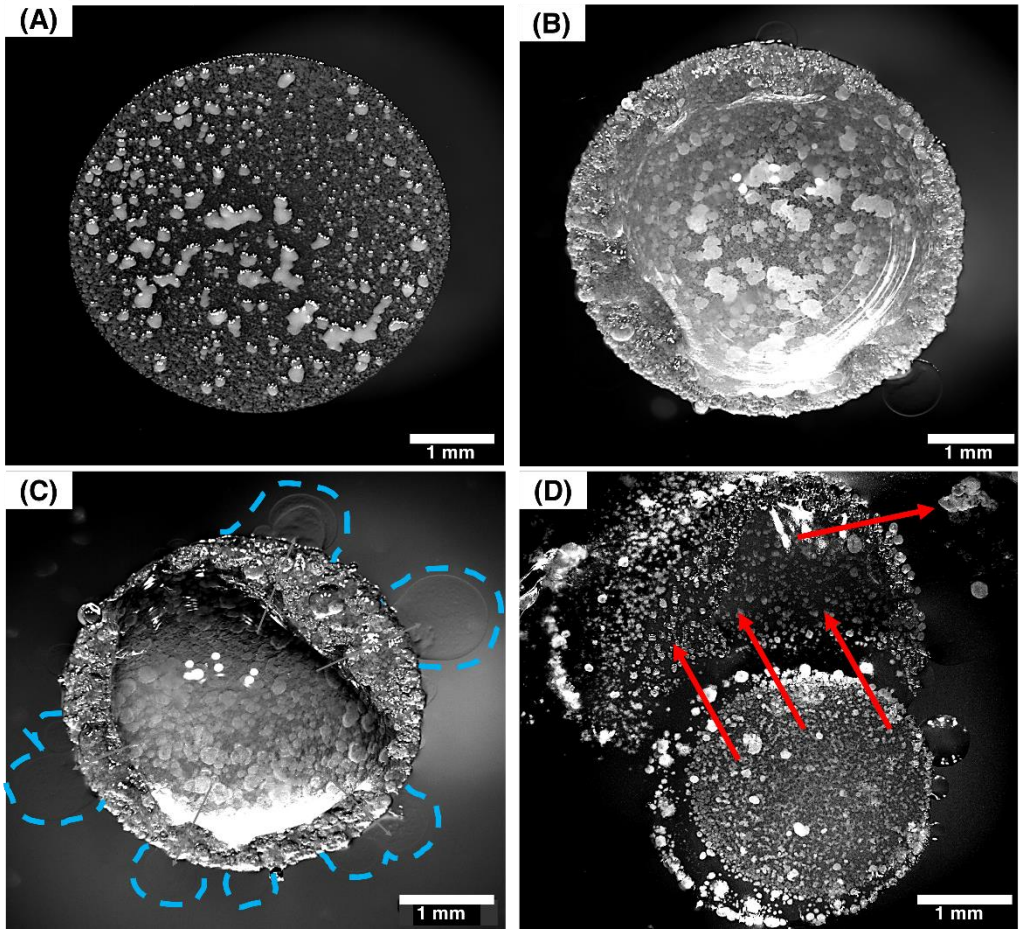

<Fig 12> *S. mutans* biofilm development under different experimental conditions following 6-day cultivation. (A) Biofilm cultured on glucose-enriched agar demonstrates the absence of EPS production or expansion. (B) Biofilm cultivated on sucrose-enriched agar exhibits EPS production without expansion. (C) Biofilm developed on sucrose-enriched agar under elevated humidity displays EPS production and spreading, yet no expansion. Blue dashed lines delineate spread EPS margins lacking new colony development. (D) Biofilm cultivated on sucrose and hydroxyapatite-enriched agar under high-humidity environments demonstrates EPS production, spreading, and consequent new colony development. Red arrows denote the stepwise progression of *S. mutans* biofilm expansion throughout 6 days. Scale bars = 1 mm

S. mutans biofilms exhibited distinct morphological differences when cultured on agar plates supplemented with either 1% sucrose or 1% glucose. From day 1, colonies grown on sucrose-supplemented media developed characteristic balloon-like EPS formations on their surfaces (Fig 13). When viewed from the side, the biofilm and the agar interface were easily distinguishable under sucrose-supplemented conditions. The formed EPS structures progressively increased into dome-shaped formations by day 6, creating protruded structures (Fig 14).

In contrast, from day 1, biofilms cultured on 1% glucose-supplemented media displayed relatively flat morphology without any visible protrusions (Fig 13). The interface between the glucose-supplemented agar and the biofilm remained less distinct compared to the sucrose condition. Throughout the 6-day observation period, no visible EPS formation or biofilm expansion was detected in glucose-supplemented conditions despite daily media replacement (Fig 15).

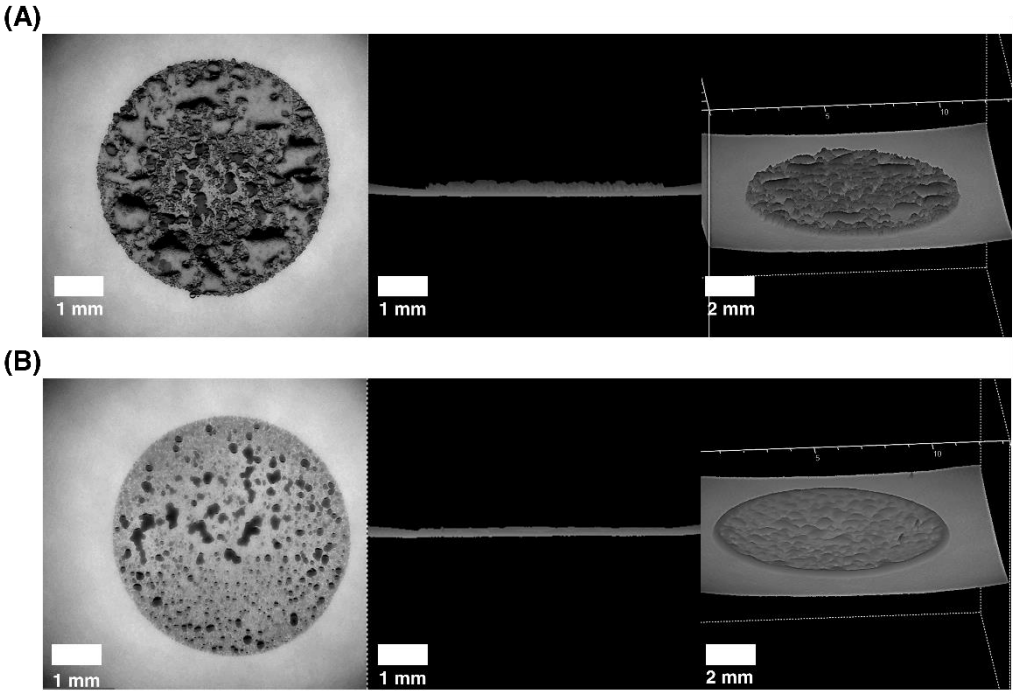

<Fig 13> Stereomicroscopic analysis of biofilms from multiple perspectives. (A) *S. mutans* biofilm under 1% sucrose conditions shows clear EPS formation, characterized by a bubble-like morphology (top view, left), a visibly thickened biofilm layer (side view, middle), and distinct bubble-like protrusions (oblique 45° view, right). (B) Biofilm under 1% glucose conditions shows no apparent EPS formation, as evidenced by a smooth surface without noticeable features (top view, left), a flat and thin biofilm layer (side view, middle), and the absence of any EPS-associated structures beyond colony formation (oblique 45° view, right). Scale bars = 1 mm (left, middle). Scale bars = 2 mm (right).

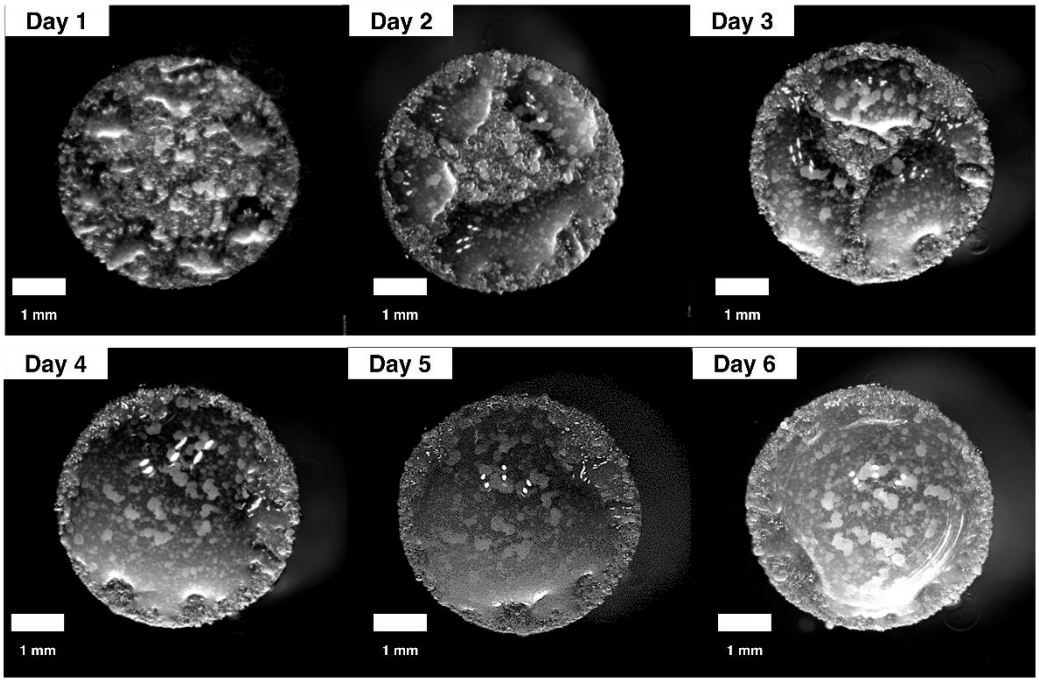

<Fig 14> Time-course stereomicroscopic images of *S. mutans* biofilm grown on sucrose-supplemented agar over a 6-day period. While colony formation and EPS formation were detected, no visible expansion of biofilm was observed. Scale bars = 1 mm.

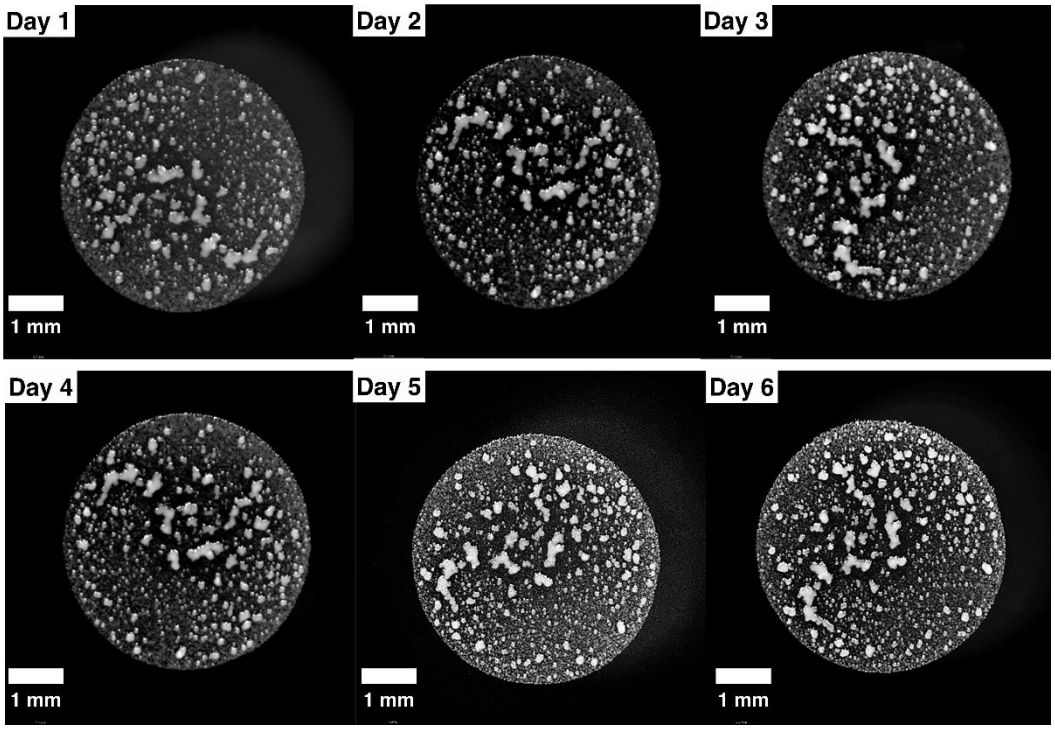

<Fig 15> Time-course stereomicroscopic images of *S. mutans* biofilm grown on glucose-supplemented agar over 6-day period. While colony formation was visible, neither EPS formation nor biofilm expansion was observed. Scale bars = 1 mm.

Fig 16 shows biofilm size measurements throughout a 6-day period on 1% sucrose or 1% glucose-supplemented agar. The quantitative analysis of biofilm expansion revealed no significant increase in colony size for either the glucose or sucrose-only conditions over the 6-day experimental period (p>0.05).

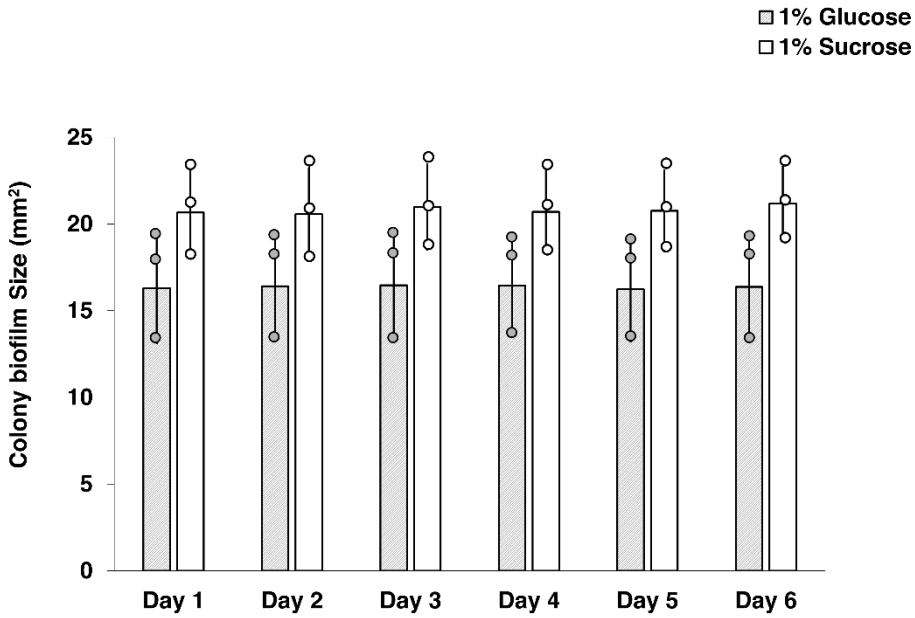

<Fig 16> Biofilm dimension analysis demonstrates no significant expansion (p>0.05) throughout 6 days in conditions containing only 1% sucrose or 1% glucose.

3.7.2 Unique expansion pattern under dental caries-mimicking conditions

When grown on medium supplemented with both 1% sucrose and 1% hydroxyapatite powder, *S. mutans* biofilms demonstrated a significant expansion compared to biofilms cultured on either sucrose-only or glucose-only supplemented MH agar plates. These biofilms expanded to more than twice their original size within a 6-day period and displayed a previously undescribed stepwise expansion pattern as summarized in Table 1. *S. mutans* biofilm expansion showed EPS matrix spreading followed by new colony formation. The overall expansion pattern is illustrated in Fig 18, which shows the cyclical nature of EPS spreading followed by new colony formation. Specifically, the EPS spread area presented dot-like particles as shown in a close-up stereomicroscopic image (Fig 19), which later became new colonies.

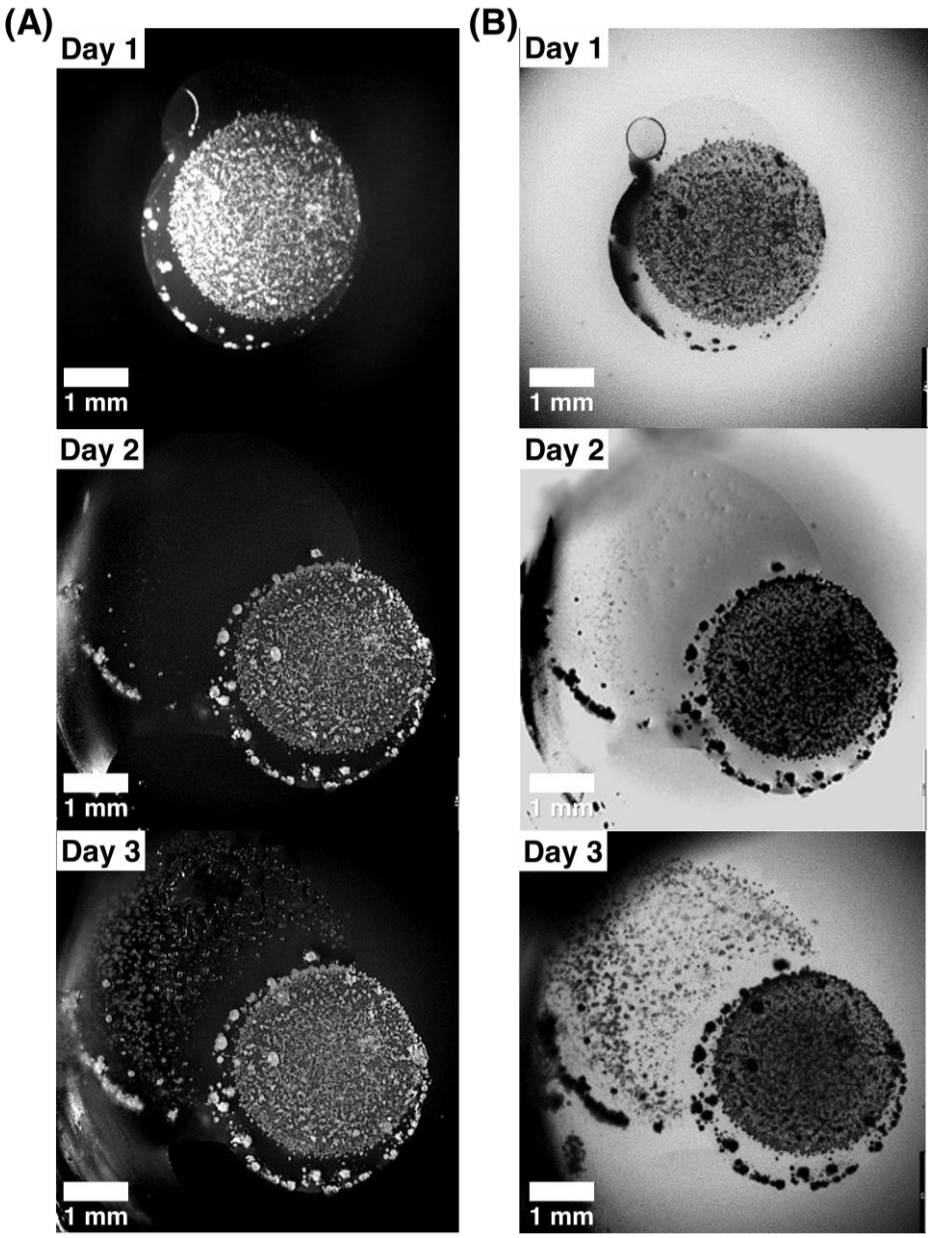

<Fig 17> Time-lapse stereomicroscope images of *S. mutans* biofilm development on sucrose- and hydroxyapatite-supplemented agar plates under elevated humidity over a 6-day incubation period (Day 1 to Day 6). The same sample was imaged daily using two illumination modes: (A) top-illumination (reflected light) and (B) bottom-illumination (transmitted light). The images presented here represent Days 1 to 3 of biofilm expansion. Scale bars = 1 mm.

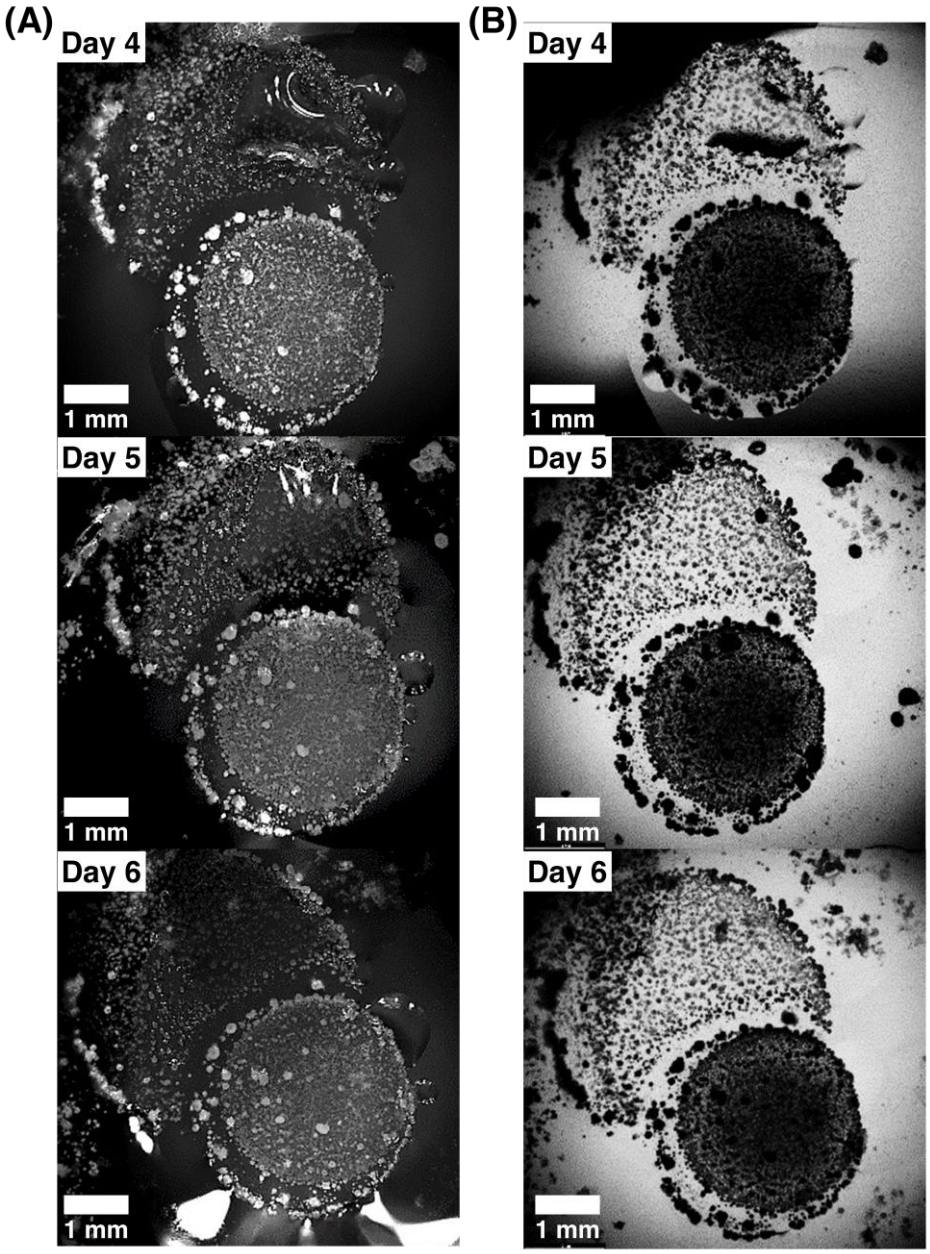

<Fig 17> (Continued) Continued time-lapse images of *S. mutans* biofilm under the same imaging conditions as above. Shown here are Days 4 through 6. Scale bars = 1 mm.

<Table 1> Temporal stages of *S. mutans* biofilm expansion under sucrose and hydroxyapatite supplemented conditions.

Time period	Key Observations
Days 1	EPS matrix formation was observed at the initial inoculation site.
Days 2	EPS from the initial colony spread onto the agar, with barely visible small dots appearing.
Days 3	Evident colony formation in EPS-spread areas, and secondary formed microcolonies beginning to produce EPS matrix.
Days 4	Newly formed microcolonies actively produce EPS and EPS matrix, starting to spread outwards into the peripheral areas of secondary-formed microcolonies.
Days 5	Prominent EPS spreads from the secondary formed biofilm, with new microcolonies starting to form.
Days 6	More microcolony formation on EPS spread areas follows the same pattern.

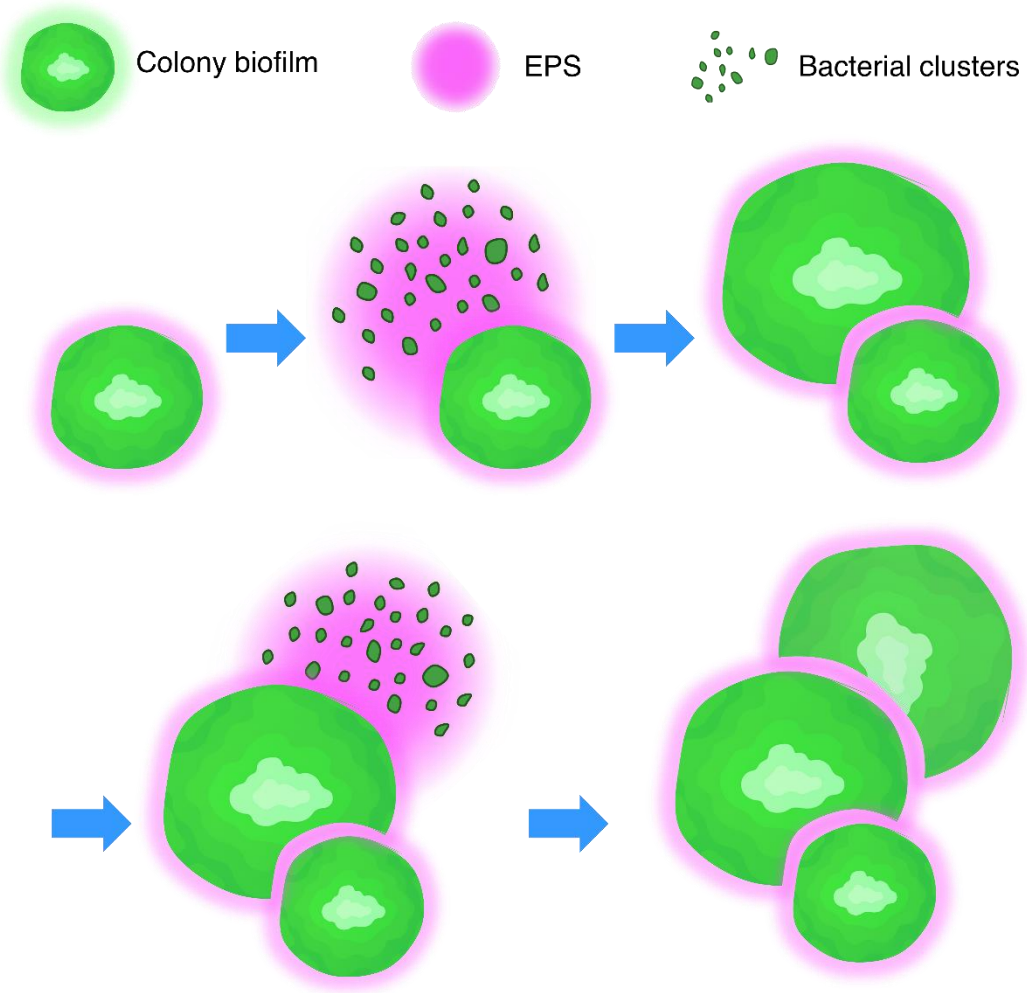

<Fig 18> Schematic illustration of *S. mutans* biofilm expansion over a 6-day period. EPS initially formed around the central colony, allowing bacterial clusters to spread to nearby areas. These clusters then developed into new colonies and produced EPS again, repeating the same process. Through this repeated cycle, the biofilm gradually expanded and, by day 6, had grown to more than twice its original size.

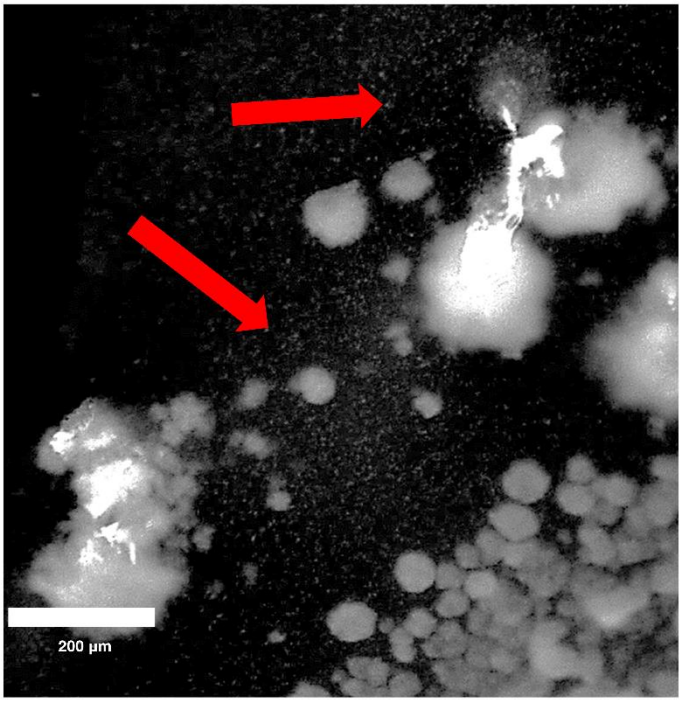

<Fig 19> Magnified view of microparticles situated between early biofilm developmental regions. Red arrows highlight bacterial clusters that first appeared as microparticles and progressively matured into microcolonies. Scale bar = 200 μm.

3.7.3. Microcolony analysis across developmental regions

To further characterize the structural features of the expanded biofilm, segmentation and color-mapping analysis were performed on the 6-day biofilm image. As shown in Fig 20 and Fig 21, based on their chronological emergence and maturation, the biofilm regions were categorized as R1, R2, and R3, corresponding to the initial inoculation site, the first expansion zone, and the subsequent region, respectively. Particle size visualization through color mapping indicated a distinct distribution pattern, with microcolonies of increased dimensions along the peripheral regions of each region, particularly in R2 (Fig 20). Due to the high bacterial density, R1 exhibited densely packed microcolonies with indistinct boundaries, making segmentation challenging. In contrast, R2 and R3 displayed more defined microcolony boundaries, enabling clearer observation. The defining features of each region, including microcolony distribution and boundary clarity, are summarized in Table 2.

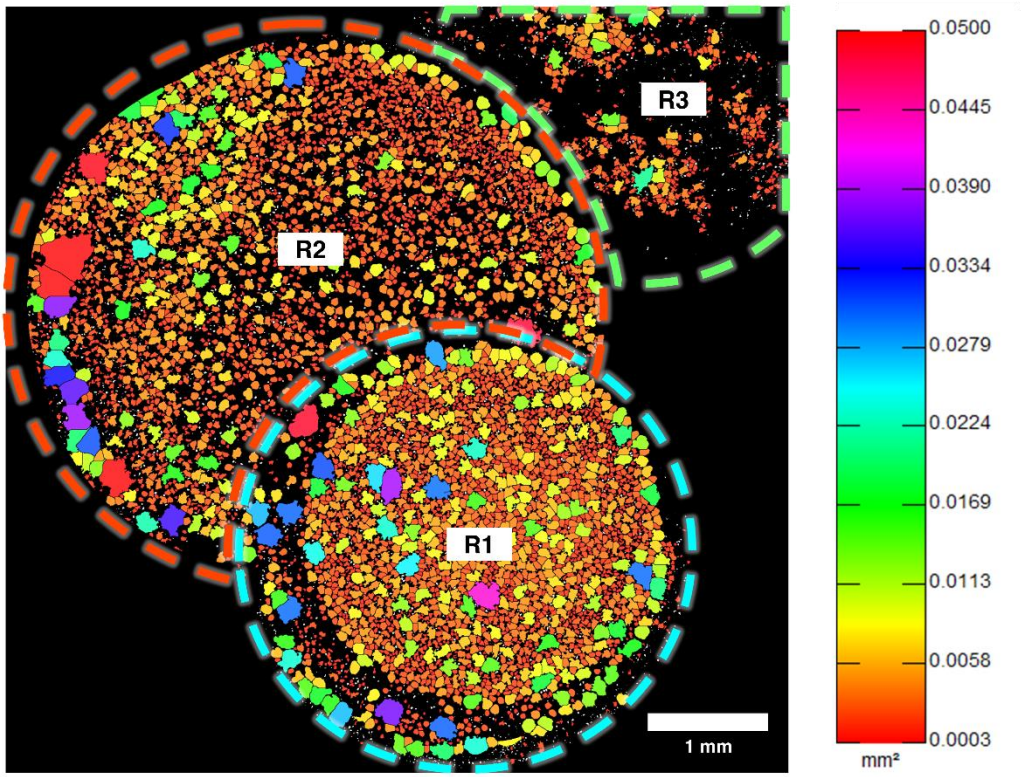

<Fig 20> Size-based color mapping of *S. mutans* biofilm at day 6 reveals microcolony distribution characteristics. Dashed boundary lines are color-coded in blue, red, and green to demonstrate regions R1, R2, and R3, respectively. Scale bar = 1 mm.

<Table 2> Regional classification and microcolony features of *S. mutans* biofilm expansion over 6 days.

Region	Formation period	Microcolony characteristics	Area coverage
R1	Initial inoculation	High packing density, obscure individual colony boundaries	77% of the biofilm area
R2	First expansion (from R1)	Increased delineation between colonies, more defined boundaries allowing precise morphology observation	33% of the biofilm area
R3	Second expansion (from R2)	Loosely clumped bacterial chains, similar to planktonic bacteria, diffuse boundaries	Not quantifiable

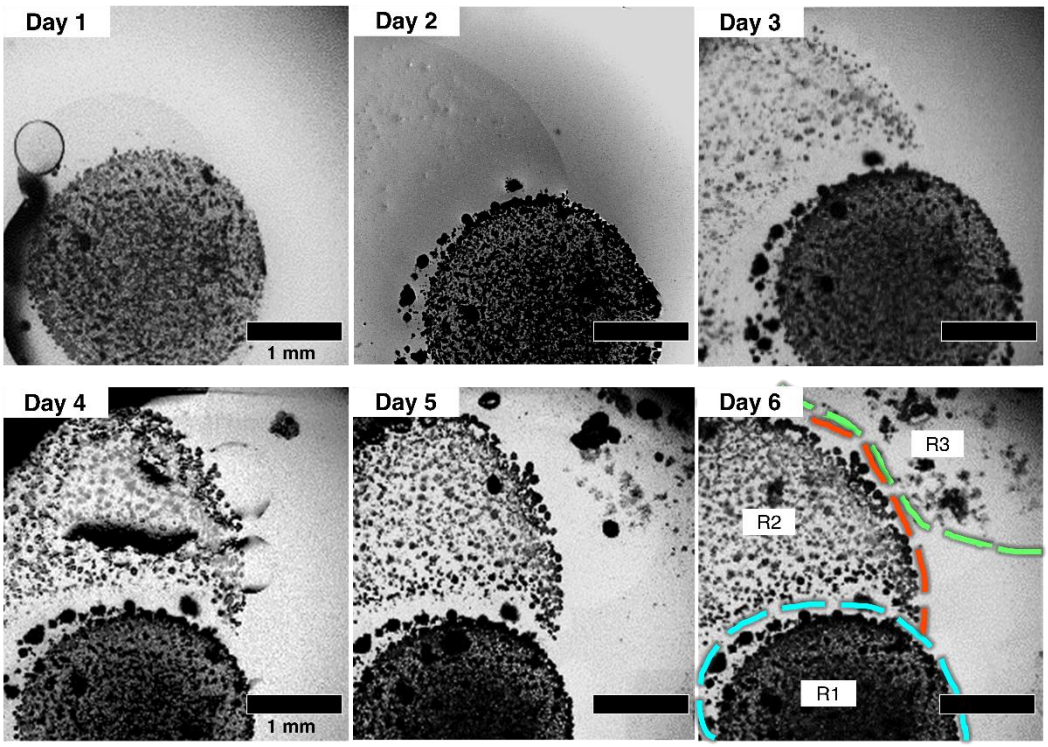

<Fig 21> Close-up stereomicroscopic images showing the temporal expansion of *S. mutans* biofilm over a 6-day period (Day 1 to Day 6). A time-lapse observation revealed lateral expansion of the biofilm, which was categorized into three distinct regions—R1, R2, and R3—based on their chronological order of appearance. R1 corresponds to the initial site of biofilm formation, whereas R2 and R3 represent subsequently formed zones of biofilm expansion observed at later time points. In the image from day 6, the boundaries of R1, R2, and R3 are delineated with blue, red, and green dashed lines, respectively, to visualize the sequential development of biofilm architecture. Scale bars = 1 mm.

3.7.4. Microcolony characteristics and biofilm expansion

ImageJ-based particle analysis was conducted to examine biofilm colonies at various time points. The relationship between total biofilm coverage area and individual microcolonies was assessed in regions R1 and R2. Due to the unclear boundaries of colonies area observed in region R3, this region was excluded from the quantitative analysis. No significant correlation was found between biofilm coverage area and microcolony count. In contrast, a positive correlation was found between individual microcolony size and percentage of biofilm coverage area (Fig 22). Based on these results, subsequent analyses focused on microcolony size rather than count.

Microcolonies exhibited distinct distribution patterns across different regions of the biofilm. Quantitative analysis was most feasible in region R2. Mean microcolony size exhibited a gradient size increase corresponding to greater distances from region R1, extending from 0.0015 mm^2 at the 0.5 mm to 0.003 mm^2 at the 3.0 mm from the R1 boundary (Fig 23).

Temporal analysis across regions R1 to R3 revealed a gradual increase in average microcolony size, accompanied by a reduction in the time required to reach maximum size. Specifically, the time to reach an average particle size of 0.003 mm^2 decreased from 5 days in R1, to 3 days in R2, and 2 days in R3 (Fig 24). These results indicate an accelerated growth pattern in later-stage regions, suggesting that microcolony development occurs more rapidly as the biofilm expands outward.

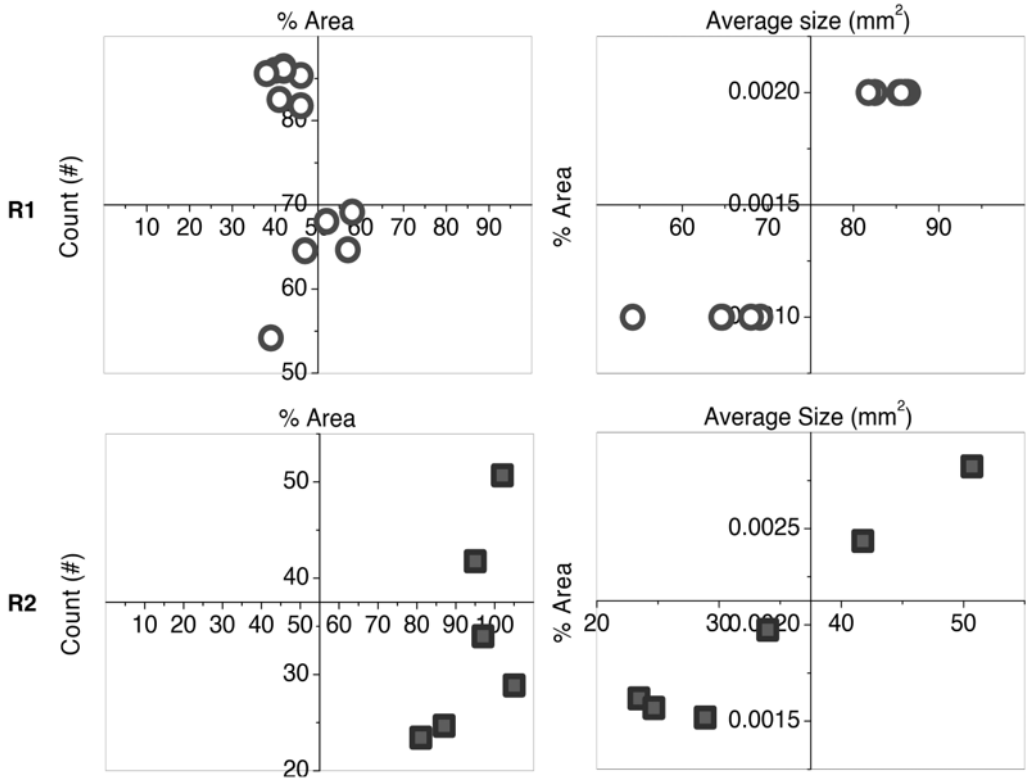

<Fig 22> Quantitative analysis of microcolony features in *S. mutans* biofilm using ImageJ software. Individual microcolonies within the biofilm were analyzed based on three parameters: size (area per colony), number (population), and relative area contribution (percentage of total biofilm area). The analysis revealed that the overall morphology and structural characteristics of the biofilm were strongly influenced by the distribution and size of individual microcolonies. Larger microcolonies occupied a greater area and contributed to the biofilm, suggesting that microcolony growth dynamics play a key role in determining biofilm size.

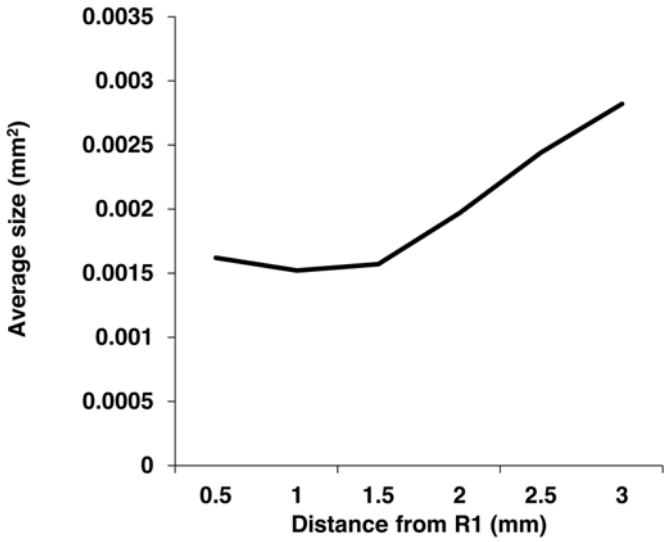

<Fig 23> Analysis of microcolonies in region R2 revealed a gradient in colony size, with larger microcolonies observed at greater distances from the initial inoculation site. This trend may be attributed to changes in the local chemical environment during biofilm expansion. As the biofilm spreads outward, alterations in nutrient distribution and pH could create favorable conditions for peripheral colony growth. In addition, the reduced bacterial population density at the expanding front may further support the development of larger microcolonies.

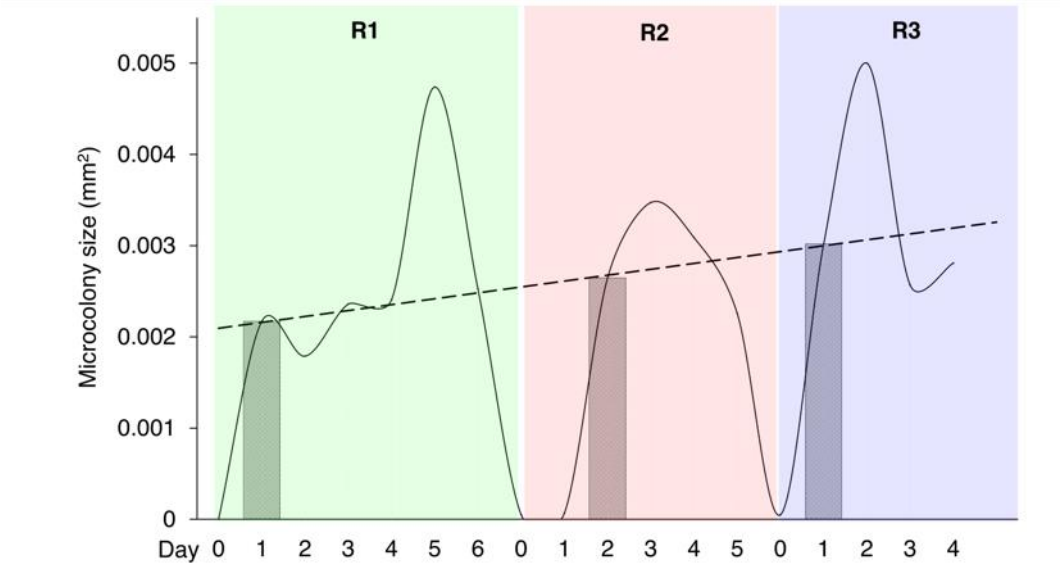

<Fig 24> Combined analysis of *S. mutans* biofilm expansion revealed a unique pattern characterized by a repetitive growth cycle. Microcolonies in regions R1, R2, and R3—classified based on their chronological emergence—showed a progressive increase in average size from R1 to R3. Moreover, the time required for microcolonies to reach their maximum size decreased sequentially across the regions, indicating accelerated growth in later-emerging areas. Notably, the transition from R1 to R2 and R2 to R3 exhibited a recurrent pattern wherein small, dot-like structures first appeared and gradually increased in size, suggesting a repeated colony formation and expansion process during biofilm development.

4. DISCUSSION

This study revealed a previously undescribed rapid expansion of non-motile *S. mutans* biofilms within the context of dental caries development. Although existing literature concerning bacterial biofilm expansion has predominantly concentrated on motile species, non-oral species, particularly those exhibiting swarming or gliding motility (Jautzus, van Gestel, and Kovács Á 2022; Kearns 2010; Yan et al. 2017; Ziege et al. 2021), this research provides an alternative process highlighting EPS-mediated expansion of a non-motile cariogenic pathogen. Unlike gliding motility-driven expansion, which involves active movement of individual cells across surfaces, *S. mutans* biofilms displayed a unique two-stage expansion strategy: initial outward spreading driven by osmotic pressure through EPS production, followed by new colony formation in neutralized environments (Fig 25). This two-stage process differs fundamentally from previously described continuous migration modes. This research utilized an experimental framework specifically constructed to mimic *S. mutans* biofilm development on tooth substrates in a simplified manner while maintaining consistent nutrient availability.

While agar plates cannot fully replicate the complex natural environment, they serve as an essential tool for studying biofilm expansion driven by osmotic pressure. These plates allow consistent control of nutrient and moisture content, ensuring experimental reproducibility. The hydroxyapatite powder incorporated into the agar plates simulated the enamel surface, as synthetic hydroxyapatite powder possesses physicochemical properties similar to natural tooth enamel (Enax and Epple 2018; Meyer et al. 2018; Pepla et al. 2014). To more mimic oral conditions, the experimental design employed an air-solid interface within a high-humidity incubator, rather than using completely immersed conditions often seen in other *S. mutans* studies (Kim, Jeon, and Kim 2018; Wang et al. 2021). This approach facilitates observation of biofilm expansion on surfaces while simulating the humid oral environment.

The use of PET membrane inserts with a 0.4 μm pore size further enhanced the physiological relevance of the model. This setup enabled regulated nutrient transfer while inhibiting bacterial translocation, consistent with earlier investigations examining osmotic pressure-influenced biofilm expansion in *Vibrio cholerae* (Yan et al. 2017). The selective permeability characteristics of the PET membrane promoted water and nutrient diffusion while establishing a stable microenvironment suitable for biofilm growth. This methodology permitted the recognition of *S. mutans* biofilm expansion that could have remained hidden in more intricate experimental systems. Additionally, the use of a PET membrane reduced the influence of acid production by *S. mutans* on agar, which could have otherwise affected the experimental results. Acid production can alter the physical properties of the agar substrate, potentially introducing unintended physical variables that may influence biofilm expansion. By incubating the *S. mutans* biofilm on PET membranes, these uncontrolled variables were effectively minimized, enabling a more accurate and reliable assessment

of the biofilm's expansion pattern.

In order to investigate the role of osmotic pressure, dextran solution was utilized as a non-biological EPS simulation system, as water-soluble glucan in *S. mutans* EPS is dextran (Lynch et al. 2007). When a high concentration of dextran solution was inoculated on agar surfaces with various concentrations, the droplet size increased within 30 minutes. The documented dextran droplet spreading corresponded with earlier results reported by Yan et al. (Yan et al. 2017). Furthermore, the increased dextral solution level in the insert further supports the osmotic water uptake of the EPS model system. Along with the abiotic EPS model system, the increased *S. mutans* biofilm mass analysis additionally confirmed water absorption from the adjacent environment. This sequence of experimental procedures revealed that glucan-enriched EPS produces an adequate osmotic force to promote matrix movement and bacterial translocation.

Further evidence was provided by confocal microscopy with green fluorescent bacteria and red fluorescent particles. Fluorescent particles with dimensions suitable for passage through a porous membrane were dispersed throughout the agar. This methodology enabled verification of osmotic water absorption by *S. mutans* EPS. The observed red fluorescent particles combined with green fluorescent bacteria appeared similar to fluorescently labeled EPS (Koo et al. 2010; Lawrence et al. 2016; Strathmann, Wingender, and Flemming 2002) from previous studies, implying red fluorescent particles embedded in the EPS matrix. The evident separation between red fluorescent particles and green fluorescent bacteria confirms the theory that osmotic forces produced by glucan within the EPS matrix result in water absorption from the agar substrate (Bowen et al. 2018; Klein et al. 2015; Koo et al. 2010).

Upon establishing the role of EPS-mediated osmotic pressure in *S. mutans* biofilm expansion, this study investigated the interaction between hydroxyapatite and its influence on this expansion process. *S. mutans* generates acid as a metabolic end product and is capable of sustaining acid synthesis even within acidic environments, resulting in enamel dissolution and consequent dental caries development (Manton and Hayes-Cameron 2013; Selwitz, Ismail, and Pitts 2007; Van Houte et al. 1991). Under acidic conditions, hydrogen ions (H+) interact with phosphate ($PO4^{3-}$) and hydroxide (OH^-) ions within the hydroxyapatite crystalline structure. This interaction results in the release of calcium (Ca^{2+}) and phosphate ions, causing hydroxyapatite powder dissolution while simultaneously neutralizing the environmental pH. This study focused on the buffering capacity of hydroxyapatite to examine how pH changes influence *S. mutans* bacterial behavior and biofilm dynamics. Understanding how hydroxyapatite modulates the microenvironment during *S. mutans* biofilm expansion provides crucial insights into the mechanisms of biofilm formation on tooth surfaces.

While planktonic *S. mutans* is known to acidify liquid media (Guo et al. 2013; Ikäläinen et al. 2024), the results confirm that *S. mutans* biofilm grown on agar surfaces also produces sufficient acid to modify the surrounding environment. In sucrose-containing conditions that facilitate acid production, the agar surrounding the biofilm turned red, indicating that acidic byproducts from the

S. mutans biofilm diffused into the surrounding area. In contrast, on hydroxyapatite-containing agar, the areas surrounding the biofilm became more transparent without showing distinct color changes. This observation suggests that hydroxyapatite in the agar dissolved in response to the acid while simultaneously neutralizing the surrounding environment. These findings demonstrate how the interaction between *S. mutans*-produced acids and hydroxyapatite creates localized environmental conditions that influence the biofilm expansion pattern.

Although *S. mutans* possesses aciduric characteristics that allow it to maintain pH homeostasis and resist acid-mediated killing (Matsui and Cvitkovitch 2010), the current findings demonstrate that its proliferation remains significantly reduced in acidic environments. Park et al. reported increased bacterial proliferation in hydroxyapatite-containing environments, further confirming that acid neutralization influences *S. mutans* growth dynamics (Park, Sutherland, and Rafii 2019).

Based on these findings, the differential outcome of *S. mutans* on various nutrients supplemented agar plates provided essential insights into biofilm formation and expansion. It was demonstrated that biofilm expansion was exclusively observed on agar plates containing both sucrose and hydroxyapatite powder over the 6-day observation period, while other conditions failed to promote biofilm expansion. Although both sucrose and glucose can support bacterial growth as carbon sources (Jurakova et al. 2023; Lemos et al. 2019), the characteristic EPS production was exclusively associated with sucrose-supplemented conditions. This selective EPS production aligns with the established understanding that *S. mutans* possesses specific metabolic pathways for sucrose utilization that are not activated by glucose (Duarte et al. 2008; Xiao and Koo 2010). The absence of biofilm expansion in glucose-containing media supports the essential role of EPS in *S. mutans* biofilm expansion. Importantly, the observation that neither sucrose nor hydroxyapatite alone was sufficient to promote biofilm expansion indicates that both EPS production and environmental modulation are necessary for *S. mutans* biofilm expansion.

Unlike previous studies of both motile and non-motile bacteria, which typically show continuous, gradual biofilm expansion on agar plates, *S. mutans* demonstrated a unique stepwise expansion pattern. This expansion pattern was characterized by the spreading of the EPS matrix, followed by colony formation. The observed process begins with initial EPS matrix formation, resembling droplets on the colony surface, followed by outward EPS flow creating new regions for colonization. The appearance of small particle-like structures within these spread EPS regions prior to visible microcolony formation provides insight into the *S. mutans* biofilm expansion and development. These particle-like structures were observed only in association with existing biofilm regions and not in other areas of the plate. This strongly suggests that they represent bacterial cells that have come from the primary biofilm rather than hydroxyapatite particles in the agar plate.

The stepwise nature of this expansion, where EPS spreads first, followed by bacterial colonization, then subsequent EPS production and further spreading, differs significantly from the continuous expansion models typically described in biofilm literature. The requirement for both sucrose and hydroxyapatite powder in the medium for this expansion pattern suggests an important

interaction between *S. mutans*' sucrose metabolism, EPS production, and the presence of hydroxyapatite that likely mimics the natural tooth environment.

A comprehensive examination of microcolony structure and arrangement offers important understanding regarding the development of *S. mutans* biofilm expansion. The transition from densely clustered microcolonies with indistinct boundaries R1 to more defined colonies in R2, and finally to structures resembling liquid broth biofilms in R3 (Kragh, Tolker-Nielsen, and Lichtenberg 2023) demonstrates the adaptive nature in *S. mutans* biofilm development. Based on this pattern of progressive changes across regions, it is theoretically possible that additional regions (R4+) with further distinct morphological characteristics might develop with extended observation periods beyond the 6 days of this study. These morphological changes across developmental zones indicate alterations in bacterial community composition, presumably arising from decreased cell density and nutrient accessibility relative to the original inoculation site (Chacón, Möbius, and Harcombe 2018; Matsushita et al. 1999).

The noted incremental increase in colony dimensions, with larger colonies appearing at greater distances from the primary colonization site, suggests an advantage for colonies in newer regions. This advantage correlates with the acid neutralization effect of hydroxyapatite identified previously from this study. It may also be attributable to decreased resource competition (Rendueles and Ghigo 2015). As validated by bacterial density measurements in the EPS matrix, the decreased cell concentration in these newer areas may provide more space for bacterial growth, accounting for the chain-like bacterial clusters found in the most mature region (R3).

The positive correlation between individual microcolony dimensions and overall biofilm coverage indicates that the development of each established microcolony substantially affects biofilm expansion within this experimental framework. This correlation indicates that biofilm expansion is not primarily driven by increasing the number of microcolonies but rather by the enlargement of existing colonies. The observation that microcolonies increase in size with increasing distance from R1 presents two possible explanations. First, some inhibitory factor from R1 may have prevented the growth of nearby microcolonies. Second, as EPS spreads outward, bacteria may not be evenly distributed, resulting in smaller bacterial populations farther from R1, which could lead to reduced competition for nutrients and, consequently, larger colony sizes.

The analysis demonstrated a progressive increase in microcolony development rate from regions R1 to R3, where later regions reached peak colony dimensions within reduced timeframes. This pattern suggests that the environment becomes increasingly favorable for new colony formation with distance from the origin. These findings offer insight into the dynamics of biofilm expansion, highlighting the importance of individual microcolony development over colony proliferation as the primary driver of biofilm coverage. The fact that bacterial growth conditions become gradually better in certain areas suggests that the factors influencing bacterial growth are not evenly distributed, but change gradually across the plate.

This study revealed that *S. mutans* employs a unique EPS-associated expansion pattern that

enables this non-motile organism to colonize surfaces effectively. Unlike motile bacteria that rely on flagella, pili, or other motility structures for surface colonization, *S. mutans* has expanded with an alternative strategy centered on EPS matrix dynamics. EPS creates an optimal microenvironment for bacterial establishment via its effective adhesive characteristics while simultaneously functioning as a nutrient storage system that maintains and provides critical resources for bacterial development (Bowen and Koo 2011; Klein et al. 2015; Koo, Falsetta, and Klein 2013; Lynch et al. 2007). The defensive and structural functions of EPS have been extensively reported in published studies. However, these results demonstrate an EPS function in enabling bacterial movement to neighboring regions through osmotic pressure-driven matrix expansion in cariogenic biofilm. The detection of living bacteria within the spreading EPS matrix provided direct evidence that this non-motile organism can indeed be transported to new colonization sites through EPS-associated processes. This is similar to biofilm expansion (Jautzus, van Gestel, and Kovács Á 2022; Yan et al. 2017), but represents the first documentation of such a process in cariogenic biofilms. The stepwise nature of this expansion pattern, where EPS spreads first, followed by bacterial colonization, fundamentally differs from the continuous migration modes seen in motile species.

These comprehensive results explain why biofilm expansion and colony formation occurred successfully under hydroxyapatite-containing conditions. The hydroxyapatite powder neutralized the acidic environment created by *S. mutans* metabolism, enabling new colony establishment. Without hydroxyapatite powder incorporation, acids produced by the biofilm (Guo et al. 2015) diffuse to neighboring areas (Hata and Mayanagi 2003), creating conditions unsuitable for new colony growth. The interaction between acid production, neutralization by hydroxyapatite, and subsequent colony formation represents a crucial mechanism underlying the unique expansion pattern observed in this study. This provides insight into how *S. mutans* overcomes the limitations of its non-motile nature to successfully colonize tooth surfaces in the oral environment.

The insights from this study reveal several promising therapeutic strategies targeting EPS-mediated biofilm expansion that may be applicable to prevent dental caries. A critical window was identified during which bacterial populations remain vulnerable within the spreading EPS matrix. Throughout this stage, the EPS matrix harbors a comparatively low bacterial count relative to the original inoculation, offering an optimal therapeutic window. This decreased cell density constitutes a susceptible population that presumably leads to reduced EPS interconnection networks (Dogsa et al. 2005). The weakened interconnections within the spreading matrix establish a more permeable architecture, indicating enhanced accessibility for antimicrobial or antibiofilm compounds during this phase, thereby inhibiting subsequent biofilm formation.

This investigation additionally reveals the crucial significance of EPS control in interrupting the cyclical development of *S. mutans* biofilm expansion. Although earlier research has concentrated heavily on the physicochemical breakdown of EPS via EPS-degrading enzymes, these results indicate that inhibiting the initial spread of EPS could be equally crucial for effective intervention. The finding that EPS spreading occurs before bacterial establishment suggests that intervention during this early phase could successfully disrupt the biofilm development process.

This study demonstrated that osmotic pressure induces water uptake by EPS, increasing its flowability. This fundamental observation could serve as a foundation for developing more effective methods to remove EPS from surfaces, potentially enhancing the efficacy of established approaches. While the findings demonstrated that pH manipulation might suppress bacterial proliferation, this strategy is not clinically feasible since acidic environments would harm dental tissues. Therefore, future therapeutic strategies should focus on the targeted removal of EPS during its early expansion phase while maintaining conditions that preserve tooth integrity.

Although this investigation offered valuable understanding of *S. mutans* biofilm expansion via EPS-facilitated bacterial translocation, numerous components of the intricate oral environment require further examination in subsequent research. Initially, the experimental framework does not completely represent host reactions, especially salivary protective systems. The introduction of saliva presents various factors, including salivary flow characteristics, protein binding events, and enzyme functions, which may impact EPS flow behaviors. Salivary circulation could modify the osmotic forces detected, whereas different salivary elements, such as antimicrobial compounds and immune proteins, might affect biofilm formation processes (Marsh et al. 2016).

Subsequently, although the single-species model delivered essential foundational data, oral biofilms commonly occur as polymicrobial communities experiencing ongoing exposure to additional bacterial species. Earlier investigations have reported substantial co-occurrence of *Candida albicans* alongside *S. mutans* in early childhood caries (Falsetta et al. 2014; Garcia et al. 2021; Lu et al. 2023; Xiao et al. 2018), indicating intricate relationships among various microbial organisms during dental caries development. The existence of additional oral microbes might considerably alter biofilm expansion dynamics via metabolic cross-talk and resource competition.

Third, although hydroxyapatite powder effectively simulates tooth enamel composition, it does not reproduce the complex structural features of actual tooth surfaces. Additionally, the dextran-based abiotic EPS model represents a simplified version of the complex EPS matrix produced by *S. mutans*. Furthermore, a previous study has shown that calcium ions promote *S. mutans* biofilm formation. When hydroxyapatite dissolves due to acid exposure, it releases calcium ions that could potentially enhance biofilm development independent of pH neutralization effects. While this study primarily focused on pH modulation as the mechanism behind improved bacterial growth in hydroxyapatite-containing environments, future research should investigate these calcium ion-mediated interactions between hydroxyapatite and *S. mutans* more comprehensively.

Despite these limitations, this single-species study established a fundamental understanding that will serve as a critical foundation for future multi-species investigations. Based on the discoveries regarding *S. mutans* biofilm expansion processes, future research should tackle both the intricacy of the oral environment and the development of specific therapeutic approaches. Further studies incorporating multi-species biofilms would improve comprehension of the complex microbial relationships within the oral cavity. Specifically, investigating the synergistic relationship between *S. mutans* and *Candida albicans* in cariogenic biofilm expansion would be particularly

valuable, given their frequent co-occurrence in severe early childhood caries as documented in numerous clinical studies (Garcia et al. 2021; Lu et al. 2023; Xiao et al. 2018).

Furthermore, the finding that osmotic pressure significantly influences biofilm expansion provides a promising pathway for enhanced removal strategies. By leveraging this phenomenon, future research could develop methods to modulate biofilm rheological properties, potentially increasing flowability to facilitate easier removal from tooth surfaces. Additionally, while osmotic pressure effects remain consistent regardless of attachment surface, the diverse surfaces available for *S. mutans* colonization in the oral cavity present a potential research opportunity. Future studies could investigate how biofilm expansion patterns vary across different oral surfaces, including natural tooth structures, restorative materials, and prosthetic surfaces. Understanding these surface-specific expansion mechanisms could inform the design of dental materials with enhanced anti-biofilm properties. These research directions could lead to more effective interventions for preventing dental caries development and progression.

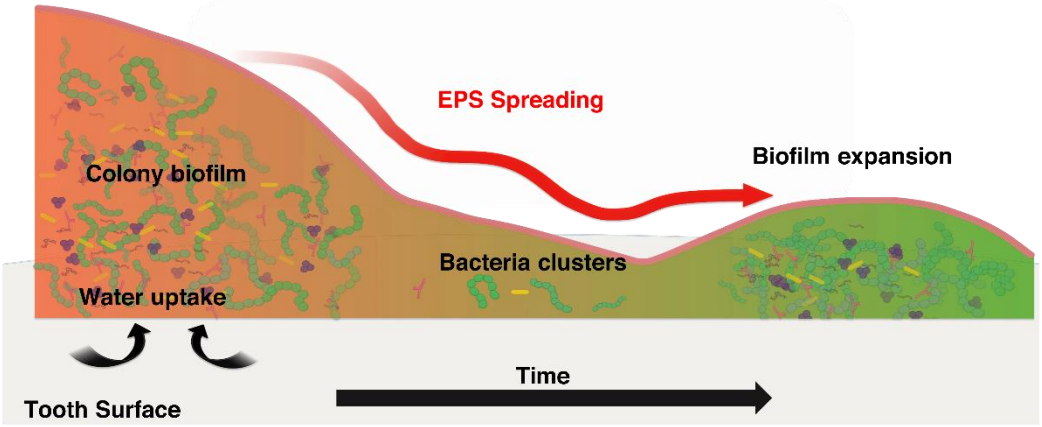

<Fig 25> Schematic illustration of osmotic pressure-driven expansion of *S. mutans* biofilm, facilitated by EPS spreading and pH neutralization. The schematic illustrates a two-stage expansion strategy of non-motile *S. mutans* biofilm on a surface. In Stage 1, sucrose metabolism induces the production of extracellular polymeric substances (EPS), creating an osmotic pressure gradient between the biofilm and the surrounding environment. This gradient drives water into the EPS matrix, resulting in the outward spreading of the biofilm. In Stage 2, acid produced by bacterial metabolism dissolves hydroxyapatite in the underlying substrate, leading to pH buffering. This neutralized microenvironment facilitates colonization by *S. mutans* cells transported within the expanding EPS, resulting in the formation of new microcolonies. This expansion, occurring in the absence of bacterial motility, represents biofilm enlargement relevant to cariogenic progression.

5. CONCLUSION

This study uncovered expansion of non-motile *S. mutans* biofilms that fundamentally differs from previously described bacterial spreading patterns. Unlike motile bacteria that rely on continuous migration, *S. mutans* employs a unique two-stage expansion strategy: initial outward spreading driven by osmotic pressure through EPS production, followed by stepwise colony formation in neutralized environments.

The osmotic pressure generated by the glucan-rich EPS matrix facilitates water uptake from the surrounding environment, creating matrix flow that enables bacterial transport to new colonization sites. This was validated through abiotic dextran model systems, biofilm weight measurements, and confocal microscopy with fluorescent particles. Viable bacteria detected within the expanding EPS matrix provided direct evidence that this non-motile organism achieves surface colonization through EPS-associated transport processes.

The interaction between *S. mutans* acid production and hydroxyapatite dissolution was crucial for biofilm expansion success. Hydroxyapatite neutralizes the acidic microenvironment created by *S. mutans* metabolism, favoring new colony establishment. This explains why biofilm expansion occurred exclusively under conditions containing both sucrose and hydroxyapatite, demonstrating that both components are necessary for the expansion process.

Microcolony analysis revealed progressive morphological changes across expansion regions, with larger colonies and accelerated maturation rates observed at greater distances from the initial inoculation site. This gradient suggests increasingly favorable growth conditions in newer regions, likely due to hydroxyapatite-mediated acid and reduced competition neutralization.

These findings reveal critical therapeutic opportunities for dental caries prevention. Understanding that EPS spread precedes bacterial colonization suggests that targeting initial EPS expansion could effectively interrupt the biofilm formation cycle. Furthermore, the osmotic pressure-driven water uptake provides a foundation for developing enhanced EPS removal strategies.

Future research should incorporate multi-species interactions and investigate the influence of salivary defense mechanisms on EPS spreading patterns. Additionally, understanding surface-specific expansion mechanisms across different oral substrates could inform the design of dental materials with enhanced anti-biofilm properties.

This research establishes EPS-mediated osmotic expansion, enabling non-motile *S. mutans* to effectively colonize tooth surfaces. These insights advance our understanding of cariogenic biofilm development and provide a scientific foundation for developing targeted therapeutic strategies that could significantly improve dental caries prevention.

References

Aframian, D. J., T. Davidowitz and R. Benoliel. 2006. "The distribution of oral mucosal pH values in healthy saliva secretors". *Oral Dis,* 12(4): 420-3.

Baker, J. L., R. C. Faustoferri and R. G. Quivey, Jr. 2017. "Acid-adaptive mechanisms of Streptococcus mutans-the more we know, the more we don't". *Mol Oral Microbiol,* 32(2): 107-117.

Beckwith, T. D. 1931. "The Bacteriology of Pulp Slime". *J Bacteriol,* 22(1): 15-22.

Berkowitz, R. J. and P. Jones. 1985. "Mouth-to-mouth transmission of the bacterium Streptococcus mutans between mother and child". *Arch Oral Biol,* 30(4): 377-9.

Berne, C., C. K. Ellison, A. Ducret and Y. V. Brun. 2018. "Bacterial adhesion at the single-cell level". *Nat Rev Microbiol,* 16(10): 616-627.

Bowen, W. H., R. A. Burne, H. Wu and H. Koo. 2018. "Oral Biofilms: Pathogens, Matrix, and Polymicrobial Interactions in Microenvironments". *Trends Microbiol,* 26(3): 229-242.

Bowen, W. H. and H. Koo. 2011. "Biology of Streptococcus mutans-derived glucosyltransferases: role in extracellular matrix formation of cariogenic biofilms". *Caries Res,* 45(1): 69-86.

Bru, J.-L., S. J. Kasallis, Q. Zhuo, N. M. Høyland-Kroghsbo and A. Siryaporn. 2023. "Swarming of P. aeruginosa: Through the lens of biophysics". *Biophysics Reviews,* 4(3).

Burne, R. A., Y. Y. Chen, D. L. Wexler, H. Kuramitsu and W. H. Bowen. 1996. "Cariogenicity of Streptococcus mutans strains with defects in fructan metabolism assessed in a program-fed specific-pathogen-free rat model". *J Dent Res,* 75(8): 1572-7.

Caufield, P. W., Y. Li and A. Dasanayake. 2005. "Dental caries: an infectious and transmissible disease". *Compend Contin Educ Dent,* 26(5 Suppl 1): 10-6.

Cawson, R. A. and E. W. Odell. 2008. "Cawson's essentials of oral pathology and oral medicine". 8th Ed. Edinburgh: Churchill Livingstone. ISBN 9780702040016; 0702040010.

Chacón, J. M., W. Möbius and W. R. Harcombe. 2018. "The spatial and metabolic basis of colony size variation". *Isme j,* 12(3): 669-680.

Cheng, L., L. Zhang, L. Yue, J. Ling, M. Fan, D. Yang, Z. Huang, Y. Niu, J. Liu, J. Zhao, Y. Li, B. Guo, Z. Chen and X. Zhou. 2022. "Expert consensus on dental caries management". *Int J Oral Sci,* 14(1): 17.

Cieplik, F., C. M. Rupp, S. Hirsch, D. Muehler, J. Enax, F. Meyer, K. A. Hiller and W. Buchalla. 2020. "Ca(2)(+) release and buffering effects of synthetic hydroxyapatite following bacterial acid challenge". *BMC Oral Health,* 20(1): 85.

Cisar, J. O., Y. Takahashi, S. Ruhl, J. A. Donkersloot and A. L. Sandberg. 1997. "Specific inhibitors of bacterial adhesion: observations from the study of gram-positive bacteria that initiate biofilm formation on the tooth surface". *Adv Dent Res,* 11(1): 168-75.

Clarke, J. K. 1924. "On the Bacterial Factor in the Ætiology of Dental Caries". *Br J Exp Pathol,* 5(3): 141-7.

Colombo, A. P. V. and A. C. R. Tanner. 2019. "The Role of Bacterial Biofilms in Dental Caries and Periodontal and Peri-implant Diseases: A Historical Perspective". *J Dent Res,* 98(4): 373-385.

Cugini, C., M. Shanmugam, N. Landge and N. Ramasubbu. 2019. "The Role of Exopolysaccharides in Oral Biofilms". *Journal of Dental Research,* 98(7): 739-745.

da Silva Bastos Vde, A., L. B. Freitas-Fernandes, T. K. Fidalgo, C. Martins, C. T. Mattos, I. P. de Souza and L. C. Maia. 2015. "Mother-to-child transmission of Streptococcus mutans: a

systematic review and meta-analysis". *J Dent,* 43(2): 181-91.
Dogsa, I., M. Kriechbaum, D. Stopar and P. Laggner. 2005. "Structure of bacterial extracellular polymeric substances at different pH values as determined by SAXS". *Biophys J,* 89(4): 2711-20.
Duarte, S., M. I. Klein, C. P. Aires, J. A. Cury, W. H. Bowen and H. Koo. 2008. "Influences of starch and sucrose on Streptococcus mutans biofilms". *Oral Microbiol Immunol,* 23(3): 206-12.
Dye, B. A., C. M. Vargas, C. D. Fryar, F. Ramos-Gomez and R. Isman. 2017. "Oral health status of children in Los Angeles County and in the United States, 1999-2004". *Community Dent Oral Epidemiol,* 45(2): 135-144.
Enax, J. and M. Epple. 2018. "Synthetic Hydroxyapatite as a Biomimetic Oral Care Agent". *Oral Health Prev Dent,* 16(1): 7-19.
Falsetta, M. L., M. I. Klein, P. M. Colonne, K. Scott-Anne, S. Gregoire, C. H. Pai, M. Gonzalez-Begne, G. Watson, D. J. Krysan, W. H. Bowen and H. Koo. 2014. "Symbiotic relationship between Streptococcus mutans and Candida albicans synergizes virulence of plaque biofilms in vivo". *Infect Immun,* 82(5): 1968-81.
Flemming, H. C. 2011. "The perfect slime". *Colloids Surf B Biointerfaces,* 86(2): 251-9.
——. 2016. "EPS-Then and Now". *Microorganisms,* 4(4).
Flemming, H. C., E. D. van Hullebusch, T. R. Neu, P. H. Nielsen, T. Seviour, P. Stoodley, J. Wingender and S. Wuertz. 2023. "The biofilm matrix: multitasking in a shared space". *Nat Rev Microbiol,* 21(2): 70-86.
Flemming, H. C. and J. Wingender. 2010. "The biofilm matrix". *Nat Rev Microbiol,* 8(9): 623-33.
Flemming, H. C., J. Wingender, U. Szewzyk, P. Steinberg, S. A. Rice and S. Kjelleberg. 2016. "Biofilms: an emergent form of bacterial life". *Nat Rev Microbiol,* 14(9): 563-75.
Fozo, E. M. and R. G. Quivey, Jr. 2004. "Shifts in the membrane fatty acid profile of Streptococcus mutans enhance survival in acidic environments". *Appl Environ Microbiol,* 70(2): 929-36.
Garcia, B. A., N. C. Acosta, S. L. Tomar, L. F. W. Roesch, J. A. Lemos, L. R. F. Mugayar and J. Abranches. 2021. "Association of Candida albicans and Cbp(+) Streptococcus mutans with early childhood caries recurrence". *Sci Rep,* 11(1): 10802.
Gibbons, R. J. and S. B. Banghart. 1967. "Synthesis of extracellular dextran by cariogenic bacteria and its presence in human dental plaque". *Arch Oral Biol,* 12(1): 11-23.
Griswold, A. R., Y. Y. Chen and R. A. Burne. 2004. "Analysis of an agmatine deiminase gene cluster in Streptococcus mutans UA159". *J Bacteriol,* 186(6): 1902-4.
Guo, L., W. Hu, X. He, R. Lux, J. McLean and W. Shi. 2013. "investigating acid production by Streptococcus mutans with a surface-displayed pH-sensitive green fluorescent protein". *PLoS One,* 8(2): e57182.
Guo, L., J. S. McLean, R. Lux, X. He and W. Shi. 2015. "The well-coordinated linkage between acidogenicity and aciduricity via insoluble glucans on the surface of Streptococcus mutans". *Sci Rep,* 5: 18015.
Hall-Stoodley, L. and P. Stoodley. 2005. "Biofilm formation and dispersal and the transmission of human pathogens". *Trends Microbiol,* 13(1): 7-10.
Hanada, N. and H. K. Kuramitsu. 1988. "Isolation and characterization of the Streptococcus mutans gtfC gene, coding for synthesis of both soluble and insoluble glucans". *Infect Immun,* 56(8): 1999-2005.
Hata, S. and H. Mayanagi. 2003. "Acid diffusion through extracellular polysaccharides produced by various mutants of Streptococcus mutans". *Arch Oral Biol,* 48(6): 431-8.
Heng, C. 2016. "Tooth Decay Is the Most Prevalent Disease". *Federal practitioner : for the health care professionals of the VA, DoD, and PHS,* 33(10): 31-33.

Hwang, G., Y. Liu, D. Kim, V. Sun, A. Aviles-Reyes, J. K. Kajfasz, J. A. Lemos and H. Koo. 2016. "Simultaneous spatiotemporal mapping of in situ pH and bacterial activity within an intact 3D microcolony structure". *Sci Rep,* 6: 32841.

Ikäläinen, H., C. Guzman, M. Saari, E. Söderling and V. Loimaranta. 2024. "Real-time acid production and extracellular matrix formation in mature biofilms of three Streptococcus mutans strains with special reference to xylitol". *Biofilm,* 8: 100219.

Jautzus, T., J. van Gestel and T. Kovács Á. 2022. "Complex extracellular biology drives surface competition during colony expansion in Bacillus subtilis". *Isme j,* 16(10): 2320-2328.

Ji, S., Y. S. Choi and Y. Choi. 2015. "Bacterial invasion and persistence: critical events in the pathogenesis of periodontitis?". *J Periodontal Res,* 50(5): 570-85.

Jones, E. M., C. A. Cochrane and S. L. Percival. 2015. "The Effect of pH on the Extracellular Matrix and Biofilms". *Adv Wound Care (New Rochelle),* 4(7): 431-439.

Jurakova, V., V. Farková, J. Kucera, K. Dadakova, M. Zapletalova, K. Paskova, R. Reminek, Z. Glatz, L. I. Holla, F. Ruzicka, J. Lochman and P. B. Linhartova. 2023. "Gene expression and metabolic activity of Streptococcus mutans during exposure to dietary carbohydrates glucose, sucrose, lactose, and xylitol". *Mol Oral Microbiol,* 38(5): 424-441.

Karygianni, L., Z. Ren, H. Koo and T. Thurnheer. 2020. "Biofilm Matrixome: Extracellular Components in Structured Microbial Communities". *Trends in Microbiology,* 28(8): 668-681.

Kearns, D. B. 2010. "A field guide to bacterial swarming motility". *Nat Rev Microbiol,* 8(9): 634-44.

Kim, M., J. Jeon and J. Kim. 2018. "Streptococcus mutans extracellular DNA levels depend on the number of bacteria in a biofilm". *Scientific Reports,* 8(1): 13313.

Klein, M. I., G. Hwang, P. H. Santos, O. H. Campanella and H. Koo. 2015. "Streptococcus mutans-derived extracellular matrix in cariogenic oral biofilms". *Front Cell Infect Microbiol,* 5: 10.

Koo, H., R. N. Allan, R. P. Howlin, P. Stoodley and L. Hall-Stoodley. 2017. "Targeting microbial biofilms: current and prospective therapeutic strategies". *Nat Rev Microbiol,* 15(12): 740-755.

Koo, H., M. L. Falsetta and M. I. Klein. 2013. "The exopolysaccharide matrix: a virulence determinant of cariogenic biofilm". *J Dent Res,* 92(12): 1065-73.

Koo, H., J. Xiao, M. I. Klein and J. G. Jeon. 2010. "Exopolysaccharides produced by Streptococcus mutans glucosyltransferases modulate the establishment of microcolonies within multispecies biofilms". *J Bacteriol,* 192(12): 3024-32.

Kragh, K. N., T. Tolker-Nielsen and M. Lichtenberg. 2023. "The non-attached biofilm aggregate". *Commun Biol,* 6(1): 898.

Krasse, B. 1965. "THE EFFECT OF CARIES-INDUCING STREPTOCOCCI IN HAMSTERS FED DIETS WITH SUCROSE OR GLUCOSE". *Arch Oral Biol,* 10: 223-6.

Kuhnert, W. L., G. Zheng, R. C. Faustoferri and R. G. Quivey, Jr. 2004. "The F-ATPase operon promoter of Streptococcus mutans is transcriptionally regulated in response to external pH". *J Bacteriol,* 186(24): 8524-8.

Larsen, T. and N.-E. Fiehn. 2017. "Dental biofilm infections – an update". *APMIS,* 125(4): 376-384.

Lawrence, J. R., G. D. Swerhone, U. Kuhlicke and T. R. Neu. 2007. "In situ evidence for microdomains in the polymer matrix of bacterial microcolonies". *Can J Microbiol,* 53(3): 450-8.

——. 2016. "In situ evidence for metabolic and chemical microdomains in the structured polymer matrix of bacterial microcolonies". *FEMS Microbiol Ecol,* 92(11).

Lemos, J. A. and R. A. Burne. 2008. "A model of efficiency: stress tolerance by Streptococcus

mutans". *Microbiology (Reading),* 154(Pt 11): 3247-3255.
Lemos, J. A., S. R. Palmer, L. Zeng, Z. T. Wen, J. K. Kajfasz, I. A. Freires, J. Abranches and L. J. Brady. 2019. "The Biology of Streptococcus mutans". *Microbiol Spectr,* 7(1).
Lu, Y., Y. Lin, M. Li and J. He. 2023. "Roles of Streptococcus mutans-Candida albicans interaction in early childhood caries: a literature review". *Front Cell Infect Microbiol,* 13: 1151532.
Lynch, D. J., T. L. Fountain, J. E. Mazurkiewicz and J. A. Banas. 2007. "Glucan-binding proteins are essential for shaping Streptococcus mutans biofilm architecture". *FEMS Microbiol Lett,* 268(2): 158-65.
Maier, B. 2021. "How Physical Interactions Shape Bacterial Biofilms". *Annu Rev Biophys,* 50: 401-417.
Manton, D. J. and L. Hayes-Cameron. 2013. "4 - Dental caries". In *Handbook of Pediatric Dentistry (Fourth Edition)*, Edited by A. C. Cameron and R. P. Widmer. Mosby. ISBN 978-0-7234-3695-9.
Manzer, H. S., A. H. Nobbs and K. S. Doran. 2020. "The Multifaceted Nature of Streptococcal Antigen I/II Proteins in Colonization and Disease Pathogenesis". *Front Microbiol,* 11: 602305.
Marsh, P. D. 2003. "Are dental diseases examples of ecological catastrophes?". *Microbiology (Reading),* 149(Pt 2): 279-294.
——. 2006. "Dental plaque as a biofilm and a microbial community - implications for health and disease". *BMC Oral Health,* 6 Suppl 1(Suppl 1): S14.
Marsh, P. D., T. Do, D. Beighton and D. A. Devine. 2016. "Influence of saliva on the oral microbiota". *Periodontol 2000,* 70(1): 80-92.
Matsui, R. and D. Cvitkovitch. 2010. "Acid tolerance mechanisms utilized by Streptococcus mutans". *Future Microbiol,* 5(3): 403-17.
Matsushita, M., J. Wakita, H. Itoh, K. Watanabe, T. Arai, T. Matsuyama, H. Sakaguchi and M. Mimura. 1999. "Formation of colony patterns by a bacterial cell population". *Physica A: Statistical Mechanics and its Applications,* 274(1): 190-199.
Meyer, F., B. T. Amaechi, H. O. Fabritius and J. Enax. 2018. "Overview of Calcium Phosphates used in Biomimetic Oral Care". *Open Dent J,* 12: 406-423.
Mira, A., A. Simon-Soro and M. A. Curtis. 2017. "Role of microbial communities in the pathogenesis of periodontal diseases and caries". *Journal of Clinical Periodontology,* 44(S18): S23-S38.
Paes Leme, A. F., H. Koo, C. M. Bellato, G. Bedi and J. A. Cury. 2006. "The role of sucrose in cariogenic dental biofilm formation--new insight". *J Dent Res,* 85(10): 878-87.
Park, M., J. B. Sutherland and F. Rafii. 2019. "Effects of nano-hydroxyapatite on the formation of biofilms by Streptococcus mutans in two different media". *Arch Oral Biol,* 107: 104484.
Pepla, E., L. K. Besharat, G. Palaia, G. Tenore and G. Migliau. 2014. "Nano-hydroxyapatite and its applications in preventive, restorative and regenerative dentistry: a review of literature". *Ann Stomatol (Roma),* 5(3): 108-14.
Pitts, N. B., D. T. Zero, P. D. Marsh, K. Ekstrand, J. A. Weintraub, F. Ramos-Gomez, J. Tagami, S. Twetman, G. Tsakos and A. Ismail. 2017. "Dental caries". *Nature Reviews Disease Primers,* 3(1): 17030.
Rathee, M. and A. Sapra. 2023. *Dental Caries*. StatPearls Publishing, Treasure Island (FL).
Reisine, S. T. and W. Psoter. 2001. "Socioeconomic status and selected behavioral determinants as risk factors for dental caries". *J Dent Educ,* 65(10): 1009-16.
Rendueles, O. and J.-M. Ghigo. 2015. "Mechanisms of Competition in Biofilm Communities". In *Microbial Biofilms*.

Saini, R., S. Saini and S. Sharma. 2011. "Biofilm: A dental microbial infection". *J Nat Sci Biol Med,* 2(1): 71-5.

Sanders, E. R. 2012. "Aseptic laboratory techniques: plating methods". *J Vis Exp,* (63): e3064.

Scannapieco, F. A. 1994. "Saliva-bacterium interactions in oral microbial ecology". *Crit Rev Oral Biol Med,* 5(3-4): 203-48.

Schilling, K. M. and W. H. Bowen. 1992. "Glucans synthesized in situ in experimental salivary pellicle function as specific binding sites for Streptococcus mutans". *Infect Immun,* 60(1): 284-95.

Schwendicke, F., C. E. Dörfer, P. Schlattmann, L. Foster Page, W. M. Thomson and S. Paris. 2015. "Socioeconomic inequality and caries: a systematic review and meta-analysis". *J Dent Res,* 94(1): 10-8.

Selwitz, R. H., A. I. Ismail and N. B. Pitts. 2007. "Dental caries". *Lancet,* 369(9555): 51-9.

Seminara, A., T. E. Angelini, J. N. Wilking, H. Vlamakis, S. Ebrahim, R. Kolter, D. A. Weitz and M. P. Brenner. 2012. "Osmotic spreading of Bacillus subtilis biofilms driven by an extracellular matrix". *Proc Natl Acad Sci U S A,* 109(4): 1116-21.

Sheiham, A. and W. P. James. 2014. "A reappraisal of the quantitative relationship between sugar intake and dental caries: the need for new criteria for developing goals for sugar intake". *BMC Public Health,* 14: 863.

Sheng, J. and R. E. Marquis. 2006. "Enhanced acid resistance of oral streptococci at lethal pH values associated with acid-tolerant catabolism and with ATP synthase activity". *FEMS Microbiol Lett,* 262(1): 93-8.

Strathmann, M., J. Wingender and H. C. Flemming. 2002. "Application of fluorescently labelled lectins for the visualization and biochemical characterization of polysaccharides in biofilms of Pseudomonas aeruginosa". *J Microbiol Methods,* 50(3): 237-48.

Takahashi, N. 2005. "Microbial ecosystem in the oral cavity: Metabolic diversity in an ecological niche and its relationship with oral diseases". *International Congress Series,* 1284: 103-112.

Trinschek, S., K. John and U. Thiele. 2016. "From a thin film model for passive suspensions towards the description of osmotic biofilm spreading". *AIMS Materials Science,* 3(3): 1138-1159.

Vacca-Smith, A. M., A. R. Venkitaraman, R. G. Quivey, Jr. and W. H. Bowen. 1996. "Interactions of streptococcal glucosyltransferases with alpha-amylase and starch on the surface of saliva-coated hydroxyapatite". *Arch Oral Biol,* 41(3): 291-8.

Van Houte, J., C. Sansone, K. Joshipura and R. Kent. 1991. "Mutans streptococci and non-mutans streptococci acidogenic at low pH, and in vitro acidogenic potential of dental plaque in two different areas of the human dentition". *J Dent Res,* 70(12): 1503-7.

Walker, G. J., A. Pulkownik and J. G. Morrey-Jones. 1981. "Metabolism of the polysaccharides of human dental plaque: release of dextranase in batch cultures of Streptococcus mutans". *J Gen Microbiol,* 127(1): 201-8.

Wang, Y., J. P. Hoffmann, S. M. Baker, K. H. Z. Bentrup, W. C. Wimley, J. A. Fuselier, J. P. Bitoun and L. A. Morici. 2021. "Inhibition of Streptococcus mutans biofilms with bacterial-derived outer membrane vesicles". *BMC Microbiol,* 21(1): 234.

Wingender, J., T. R. Neu and H.-C. Flemming. 1999. "What are Bacterial Extracellular Polymeric Substances?". In *Microbial Extracellular Polymeric Substances: Characterization, Structure and Function*, Edited by J. Wingender, T. R. Neu and H.-C. Flemming. Berlin, Heidelberg: Springer Berlin Heidelberg. ISBN 978-3-642-60147-7.

World Health Organization, W. 2022. *Global oral health status report: towards universal health coverage for oral health by 2030*. World Health Organization. ISBN 9240061487.

Xiao, J., X. Huang, N. Alkhers, H. Alzamil, S. Alzoubi, T. T. Wu, D. A. Castillo, F. Campbell, J. Davis, K. Herzog, R. Billings, D. T. Kopycka-Kedzierawski, E. Hajishengallis and H. Koo. 2018. "Candida albicans and Early Childhood Caries: A Systematic Review and Meta-Analysis". *Caries Res,* 52(1-2): 102-112.

Xiao, J. and H. Koo. 2010. "Structural organization and dynamics of exopolysaccharide matrix and microcolonies formation by Streptococcus mutans in biofilms". *J Appl Microbiol,* 108(6): 2103-13.

Yan, J., C. D. Nadell, H. A. Stone, N. S. Wingreen and B. L. Bassler. 2017. "Extracellular-matrix-mediated osmotic pressure drives Vibrio cholerae biofilm expansion and cheater exclusion". *Nature Communications,* 8(1): 327.

Zeng, L. and R. A. Burne. 2013. "Comprehensive mutational analysis of sucrose-metabolizing pathways in Streptococcus mutans reveals novel roles for the sucrose phosphotransferase system permease". *J Bacteriol,* 195(4): 833-43.

Ziege, R., A. M. Tsirigoni, B. Large, D. O. Serra, K. G. Blank, R. Hengge, P. Fratzl and C. M. Bidan. 2021. "Adaptation of Escherichia coli Biofilm Growth, Morphology, and Mechanical Properties to Substrate Water Content". *ACS Biomater Sci Eng,* 7(11): 5315-5325.

Abstract in Korean

EPS 삼투압 거동 및 수산화인회석 상호작용이 *Streptococcus mutans* 생물막 확장에 미치는 영향

치아우식증은 전 세계적으로 모든 연령층에 영향을 미치는 중대한 공중보건 문제로 자리 잡고 있다. *Streptococcus mutans* (*S. mutans*)는 치아우식증의 발생에 핵심 역할을 하는 주요 원인균으로 널리 알려져 있으나, 비운동성 세균인 이 균주가 치아 표면에서 빠르게 집락화하고, 우식성 생물막을 형성하는 기전은 지금까지 충분히 규명되지 않았다. 이전 연구에서는 운동성 및 비운동성 세균의 생물막이 삼투압에 의해 주변으로 확장될 수 있음을 보였다. 본 연구는 *S. mutans* 생물막의 삼투압 매개 확장 양상을 분석하고, 치아 표면 전반으로의 공간적 확장에 기여하는 주요 물리적 및 화학적 인자를 규명하고자 하였다.

S. mutans 생물막 내 세포 외 고분자 물질(EPS)에 의한 삼투효과를 분석하기 위해 덱스트란 용액을 활용한 비생물학적 모델 시스템을 적용하였고, 형광 나노입자를 이용하여 생물막 기질 안으로의 수분 이동을 추적하였다. 또한, *S. mutans* 의 산 생성으로 인한 pH 변화를 측정하였고, 다양한 산성 조건에서의 부유 상태의 세균 성장 분석을 통해 산성 환경 및 수산화인회석(hydroxyapatite)이 세균 성장 및 군집 형성에 미치는 영향을 평가하였다. *S. mutans* 생물막을 다양한 영양 조건하에서 특성화하기 위해 1% 포도당(glucose), 1% 자당(sucrose) 또는 1% 자당과 1% 수산화인회석이 첨가된 한천 배지 상에 반투과성 막을 위치시킨 공기-고체 계면 모델을 활용하였다. 생물막의 발달은 실체현미경과 이미지 분석을 통해 6 일 동안 평가하였으며, 생물막의 확장 양상, 세포 외 고분자 물질(EPS) 생성, 미세 군집 형성을 분석하였다.

연구 결과, *S. mutans* 생물막은 기존에 알려진 다른 세균 종의 확장 방식과는 달리, 두 단계의 독특한 방식으로 확장됨을 확인하였다. EPS 모사 실험 결과, 주변 한천 배지로부터의 수분 흡수로 인한 덱스트란 용액의 높이 증가와 확산이

관찰되었으며, 이는 EPS 의 외부 유동을 유도하기에 충분한 삼투압이 형성되었음을 시사하였다. 또한, EPS 기질 내에서 생존 가능한 세균의 존재를 확인하였고, 해당 기질이 세균을 새로운 위치로 운반하는 역할을 수행함을 입증하였다.

부유 상태의 성장 분석에서는 pH 6.5 이하에서 세균의 성장이 현저히 억제되었고, 이는 수산화인회석에 의한 완충이 *S. mutans* 생물막의 안정적인 군집 형성에 필수적임을 보여주었다. *S. mutans* 생물막의 확장 양상 분석 결과, 자당과 수산화인회석을 모두 포함한 배지에서 배양한 생물막만이 빠른 확장을 보였으며, 6 일 이내에 초기 크기의 두 배 이상으로 증가하였다. 반면, 포도당 또는 자당만 포함된 배지에서는 매일 배지를 교체하였음에도 불구하고 유의미한 확장을 보이지 않았다. 자당과 수산화인회석이 모두 포함된 조건에서는 삼투압에 의해 EPS 기질이 외부로 확산되고, 이후 수산화인회석이 포함된 환경에서 새로운 군집 형성이 이루어졌다. 생물막 내 미세 군집 분석 결과 초기 접종 부위로부터 거리가 증가함에 따라 형태학적 차이가 뚜렷하게 나타났다. 군집의 크기는 경계로부터 0.5 mm 지점에서 약 0.0015 mm^2 , 3.0 mm 지점에서는 약 0.003 mm^2 로 증가하였고, 거리 증가에 따라 성장 환경이 점진적으로 개선되었음을 확인하였다.

결론적으로, 본 연구는 *S. mutans* 생물막이 삼투에 의한 EPS 기질 확산과 그에 이은 수산화인회석 함유 환경에서의 새로운 군집 형성을 통해 확장되는 새로운 두 단계 확장 과정을 제시하였다. 이러한 확장 양상은 기존 생물막 발달 기전과는 상이하며, 자당이 풍부한 환경에서 비운동성 *S. mutans* 생물막이 치아 표면에 빠르게 집락화하는 기전을 설명할 수 있다. 또한, EPS 의 삼투 특성과 환경 pH 조절의 필수적인 역할은 우식성 생물막의 거동에 대한 새로운 통찰을 제공하며, EPS 를 표적으로 하는 예방 및 치료 전략 개발에 추가적인 과학적 근거를 제시하였다. 본 연구는 우식성 생물막의 발달에 대한 이해를 심화시키고, 치아우식증의 효과적인 예방 전략 수립에 기여할 수 있을 것으로 기대된다.

핵심되는 말 : 치아우식성 생물막, *Streptococcus mutans*, 생물막 확장, 세포외고분자물질 (EPS), 삼투압